Environmental Technology & Innovation 40 (2025) 104427

Contents lists available at ScienceDirect

Environmental Technology & Innovation

journal homepage: www.elsevier.com/locate/eti

Phenol adsorption performance by bamboo activated carbon produced using fabricated two-in-one carbonization activation pilot reactor

Mariam Jamilah Mohd Fairus [a,b], Mohamad Faizal Ibrahim [a,b,*], Nahrul Hayawin Zainal [c], Suraini Abd-Aziz [b], Lai-Yee Phang [b]

[a] Nanomaterials Synthesis and Characterisation Laboratory, Institute of Nanoscience and Nanotechnology, Universiti Putra Malaysia, 43400 UPM Serdang, Selangor, Malaysia
[b] Department of Bioprocess Technology, Faculty of Biotechnology and Biomolecular Sciences, Universiti Putra Malaysia, 43400 UPM Serdang, Selangor, Malaysia
[c] Biomass Technology Unit, Engineering & Processing Division, Malaysian Palm Oil Board (MPOB), No.6 Persiaran Institusi, 43000 Bandar Baru Bangi, Kajang, Selangor, Malaysia

ARTICLE INFO

Keywords:
Carbonization
Activation
Pilot scale reactor
Bamboo activated carbon
Pollutant removal

ABSTRACT

Phenol contamination from industrial effluents poses significant risks to ecosystems and human health. The permissible limit for phenol levels in wastewater sets by the Malaysia Environmental Quality Act of 1974 is 1 mg L^{-1} (Standard B). Therefore, this study produced bamboo activated carbon (BAC) using a pilot-scale of two-in-one carbonization and activation reactor and tested for phenol removal. BAC was carbonized at 500°C for 2 h, followed by physical activation at 800°C for 2 h. The resulting BAC demonstrated a remarkable surface area of 1018 m^2 g^{-1} , a high microporosity exceeding 80 %, and a minor presence of mesoporosity with a pore diameter of 2.08 nm. These characteristics greatly enhanced phenol removal, with BAC achieving over 90 % removal within 15 min at 0.4 g dosage, whereas commercial BAC reached only 82.4 % at the same dosage after 60 min. Additionally, BAC remained effective across a wide pH range of 2–10. The adsorption followed pseudo-first-order kinetics (R^2 = 0.9995, χ^2 = 0.0049) and multilayer adsorption as per the Freundlich isotherm model (R^2 = 0.9588, χ^2 = 0.9119). These results demonstrate the high potential of BAC produced from this reactor for effective phenol removal, with potential applications for other pollutants.

1. Introduction

Phenolic compounds materialized in the effluents of various industries such as oil refining, petrochemicals, pharmaceuticals, paper, and wood products. Disposing of untreated phenolic substances directly into the environment poses a fatal health hazard to humans, animals, and aquatic ecosystems (Mohammadi et al., 2015; Sun et al., 2015). According to the Department of Environment (DOE), 195 rivers in Malaysia are categorized as slightly polluted and 34 as polluted, based on general pollution indicators. In Selangor alone, 30 rivers are slightly polluted, while three fall under the polluted category. Notably, the concentration of phenolic compounds in several

* Corresponding author at: Nanomaterials Synthesis and Characterisation Laboratory, Institute of Nanoscience and Nanotechnology, Universiti Putra Malaysia, 43400 UPM Serdang, Selangor, Malaysia.
E-mail address: faizal_ibrahim@upm.edu.my (M.F. Ibrahim).

https://doi.org/10.1016/j.eti.2025.104427
Received 15 April 2025; Received in revised form 6 July 2025; Accepted 2 August 2025
Available online 5 August 2025

rivers, including the Klang River, Sungai Selangor, and Langat River, has been reported to exceed the permissible limits set by the Industrial Effluent Regulations 2009 for Standard A (0.001 mg L^{-1}) and Standard B (1 mg L^{-1}) with detected levels ranging from 5 to 6 mg L^{-1} (Ahmad Juanda et al., 2023; Department of Environment, 2020). Phenol particularly has been recognized as a priority pollutant by the US Environmental Protection Agency (EPA) and Canada National Pollutant Release Inventory (NPRI) (Environment and Climate Change Canada ECCC, 2022; Environmental Protection Agency (EPA), 2023) Globally, strict phenol discharge thresholds have been established with a standard discharge of < 1 ppb into the water body authorized by the EPA (Sun et al., 2015; Kazemi et al., 2014). Phenol can be eliminated through various techniques including conventional methods such as steam distillation, adsorption, and biological treatment, as well as advanced technologies such as electrochemical oxidation, photo-oxidation, and membrane processes (Villegas et al., 2016). Adsorption is commonly preferred, and various adsorbents, including pomegranate peel carbon, have been examined for their effectiveness in removing phenol from aqueous solutions (Afsharnia et al., 2016; Pradeep et al., 2015). Technology advancement for phenol treatment remains an active area of research, focusing on improving the efficiency and cost-effectiveness of removal methods (Saputera et al., 2021).

Bamboo is a renewable resource that has been widely recognized for its diverse applications. One of its significant uses is its potential to be converted into AC for wastewater treatment. The potential of bamboo as a bioadsorbent has been highlighted in the United Nations' sustainable development goals (SDGs), particularly in SDG 7, as part of national climate change strategies (Chaowana, 2013). In 2020, Malaysia introduced the National Bamboo Policy as part of the National Bamboo Industry Development Action Plan 2021–2030. This policy focuses on sustainable bamboo management, socioeconomic development, and environmental conservation. BAC production is an attractive alternative to petroleum and wood-based charcoal due to the low cost and fast growth of bamboo compared to other tree species (Bernama, 2023). Currently, most of the literature on the production of BAC focuses on laboratory-scale experiments. These experiments utilize a tube furnace along with chemical impregnation and surface modification to produce high-quality AC for effective pollutant removal (Xing et al., 2012; Zulkurnai et al., 2017; Yu et al., 2020). Previous literature describes BAC production as involving separate carbonization and activation steps with complex chemical impregnation. This process is undesirable due to increased energy consumption, equipment, labour, processing time, and environmental hazards (Moliner et al., 2022; Pal et al., 2020; Yorgun and Yıldız, 2015). This study highlights the application of the fabricated pilot-scale two-in-one carbonization and activation reactor for the production of high-quality bamboo activated carbon (BAC), aimed at achieving superior phenol removal performance. The novelty of this research lies in utilizing the fabricated reactor system, previously employed in only one other study to produce oil palm kernel shell activated carbon (OPKS-AC) with a specific surface area of 935 m^2 g^{-1}, which achieved 90 % pollutant removal from palm oil mill effluent (POME) within 12 h treatment time (Nahrul Hayawin et al., 2018). To ensure optimal performance, a tube furnace was initially used in a lab-scale preliminary study to refine the carbonization and activation parameters for BAC production. These optimized conditions were subsequently implemented in the two-in-one reactor system to assess the characteristics of the resulting BAC. The study further investigates its potential for phenol removal through comprehensive kinetic and isotherm analyses, underscoring the importance and uniqueness of this approach in advancing sustainable water treatment solutions.

2. Materials and methods

2.1. Reagents

A phenol stock solution (1 g L^{-1}) was prepared using phenol (Sigma Aldrich, USA) and stored in a dark cabinet to prevent degradation. The pH of the solution was adjusted using 0.1 M hydrochloric acid (HCl) (Merck, Germany) and 0.1 M sodium hydroxide (NaOH) (Merck, Germany). All reagents were of analytical grade to ensure experimental accuracy. Commercial bamboo activated carbon, purchased from BT Science Sdn. Bhd. (Selangor, Malaysia), was used as a control in the batch adsorption study to evaluate phenol removal efficiency.

2.2. Material preparation

Raw bamboo *(Dendracalamus asper)* collected from Beranang, Selangor was air-dried for a week before being cut into chipped sizes of 5 × 2 cm and 1 × 1 cm. The bamboo chips were then further dried in the oven for 24 h at 105°C to reduce the moisture content to less than 10 % before further use. The thermal stabilities and proximate analysis of the raw bamboo were conducted by thermogravimetric analysis/differential scanning calorimetry (TGA/DSC) (Mettler-Toledo, USA) at a heating rate of 5°C min^{-1} under inert conditions (Zulkurnai et al., 2017). The lignocellulosic composition of raw bamboo was determined based on the Technical Association of the Pulp and Paper Industry (TAPPI) standard method (Ioelovich, 2015).

2.3. Bamboo activated carbon production

2.3.1. Carbonization and activation optimisation using tube furnace

In this study, the carbonization and activation conditions were optimized by using tube furnace in a lab scale-study. Approximately 20 g of dried bamboo chips, measuring 5 × 2 cm was then subjected to carbonization at temperatures ranging from 300°C to 700°C, with holding times varied between 1 and 4 h. The carbonization optimization condition of bamboo charcoal (BC) was conducted under an inert condition with a nitrogen flow rate of 500 mL min^{-1} and a heating rate of 40°C min^{-1} by a tube furnace (Wang et al., 2013). BC prepared were labelled as BC300–1 for instance, which referred to their activation temperature of 300°C and holding time of 1 h. After the carbonization condition was optimized, the activation was carried out where the activation temperatures were varied from 700 to

1000°C with a holding time of 1–4 h simultaneously. Activation was conducted under CO_2 gas flow which was set to 300 mL min^{-1} with a heating rate of 20°C min^{-1} (Wang et al., 2013). BAC produced were labelled as BAC800–1 which represented their activation temperature and holding time during activation.

2.3.2. Carbonization and activation using two-in-one reactor

The optimized carbonization and activation conditions established in lab-scale study were upscaled in two-in-one carbonization-activation. Raw bamboo chips of 3 kg were loaded into the reactor chamber for simultaneous carbonization and activation. The reactor, designed with a double-insulated system made from low-cement castable reinforced with alkaline-resistant organic fibers and encased in stainless steel plating, can withstand temperatures up to 1440°C (Nahrul Hayawin et al., 2018). Carbonization was conducted under a nitrogen atmosphere at a flow rate of 500 mL min^{-1} and a heating rate of 40°C min^{-1}, followed by steam activation at a controlled flow rate of 22.77–26.02 mL min^{-1}. Steam, generated at 170°C, was purged into the system in every 30 s intervals with 30 s resting periods throughout the activation process. After activation, the steam supply was stopped, and the reactor was cooled to below 100°C using a blower (Nahrul Hayawin et al., 2018). The resulting activated carbon was unloaded and collected for subsequent analyses. The textural characteristics of the BAC produced from the pilot-scale study were then evaluated.

2.4. Characterization of bamboo charcoal and bamboo activated carbon

The textural characteristics of BAC were determined according to the nitrogen adsorption-desorption isotherms at 77 K by a volumetric adsorption analyzer (Quantrachrome Autosorb-iQ-C, Anton Paar, USA). The Brunauer-Emmett Teller (BET) was applied to calculate the specific surface area meanwhile total pore volume and average pore size were calculated by the t-plot method (Barrett et al., 1951; de Almeida et al., 2019). The surface morphologies and chemical compositions of the BAC produced were analysed scanning electron microscopy-energy dispersive X-ray spectroscopy (SEM-EDX) (Hitachi S-3400 N, Japan). The images were obtained with a working voltage of 12 kV and magnification of 500x and 2.00k (de Almeida et al., 2019). The surface functional group of the BAC produced was determined using Fourier-transform infrared spectroscopy (FTIR) (TG-IR Hypernation System, Perkin Elmer, USA) with a resolution of 4 cm^{-1} in the range from 4000 to 500 cm^{-1} (de Almeida et al., 2019). Proximate analysis and thermal degradation of the BAC were obtained by using thermogravimetric analysis (TGA) (Mettler Toledo TGA/SDTA 851, USA) with a heating rate of 25°C min^{-1} under a N_2 flow with a rate of 50 mL min^{-1} until 800°C (de Almeida et al., 2019)

2.5. Batch adsorption study of phenol removal

The method used in this experiment was adapted from Ge et al. (2018) with modifications. A batch adsorption test was conducted by introducing a known weight of BAC into a 100 mL conical flask containing 50 mL of 0.1 g L^{-1} phenol solution with adjusted pH 7. The flasks were shaken in an incubator shaker (Benchmark Scientific, Incu-Shaker 10 L, USA) at 180 rpm at room temperature for up to 210 min. The parameters studied were contact time (5–210 min), adsorbent dosage (0.1–0.5 g, equivalent to 2–10 g L^{-1} in a 50 mL working volume) and pH (2−12). After shaking, sample solutions were filtered using a syringe filter of 22 μm. A commercial BAC was used as a control, where a selected set of conditions for phenol removal using commercial BAC was applied to evaluate the efficiency of BAC800–2. The determination of phenol concentration was conducted using an ultraviolet-visible spectrophotometer (OPTIZEN POP, Korea) at 270 nm with quartz cuvettes (Ge et al., 2018). The standard curve was also plotted by preparing phenol solutions with concentrations ranging from 0.01 to 0.10 g L^{-1}. All results presented in this study were obtained from triplicate experiments, and the lab work was conducted repeatedly to ensure data accuracy and replicability. The percentage removal (%) and amount of phenol adsorbed, the adsorption capacity at the time, q_t (mg g^{-1}) and the adsorption capacity at equilibrium, q_e (mg g^{-1}), are determined by using Eqs. 1, 2 and 3, respectively.

$$\text{Removal efficiency}(\%) = [(C_O - C_e)/(C_O)] \times 100 \quad (1)$$

$$q_t = (C_O - C_t)V/m \quad (2)$$

$$q_e = (C_O - C_e)V/m \quad (3)$$

where C_o, C_t and C_e (mg L^{-1}) are the concentration of phenol at initial, time and equilibrium respectively. Meanwhile, V (L) is the volume of the solution, and m (g) is the mass of BAC used.

2.6. Point of zero charge (pH_{pzc})

The point of zero charge (pH_{pzc}) refers to the pH at which a material's surface charge is neutral, and all active sites are uncharged. In this study, the pH_{pzc} of was determined using the salt addition method. Specifically, 0.05 g of BAC was added to 10 mL of a 0.01 M NaCl solution in a 100 mL conical flask, and the pH was adjusted to a range of 2–12 using 0.1 M NaOH or HCl. The flasks were shaken for 24 h, after which the final pH values were recorded. The difference between the initial and final pH (ΔpH) was calculated, plotted against the initial pH, and the pH_{pzc} was identified from the point of intersection with the pH axis (Dawodu et al., 2019).

2.7. Kinetic modelling

Kinetic phenol adsorption onto BAC was performed to investigate the efficiency of the adsorbate uptake on the adsorbents and the adsorption process design by using Origin 2019b software version 9.6.5 (OriginLab Corporation, Northampton, Massachusetts, USA) and the Nonlinear Curve Fit Tool. The kinetic parameters were acquired by fitting the experimental data to several types of kinetic models, which are pseudo-first-order (PFO) (Lagergren, 1898), pseudo-second-order (PSO) (Ho, 1995) and Elovich (Cheung et al., 2000) are presented by Eqs. 4, 5 and 6, respectively.

$$q_t = q_e(1 - e^{-k_1 t}) \tag{4}$$

$$q_t = \frac{q_e^2 k_2 t}{1 + q_e k_2 t} \tag{5}$$

$$q_t = \frac{1}{\beta}\ln(\alpha\beta) + \frac{1}{\beta}\ln(t) \tag{6}$$

Besides, the intraparticle diffusion (IPD) model (Weber and Morris, 1963) denoted by Eq. 7 was applied to explore the possibility of IPD resistance affecting adsorption behaviour and to evaluate the rate-controlling steps involved in the adsorption process.

$$q_t = k_3 t^{0.5} + C \tag{7}$$

Where k_1 (1 min^{-1}), k_2 (g (mg min)$^{-1}$) and k_3 (mg (g min)$^{-0.5}$) is the rate constant of PFO, PSO, and IPD respectively. C (mg g^{-1}) is the constant associated with the thickness of the boundary layer and α ((mg g^{-1}) min) and β (g mg^{-1}) are the initial adsorption rate and desorption rate, respectively.

2.8. Isotherm modelling

Isotherm models are essential in demonstrating the equilibrium limitations of the adsorption system. Three isotherm models, namely the Langmuir (Langmuir, 1916) Freundlich (Freundlich, 1906) and Temkin (Temkin and Pyzhev, 1940) were adopted to fit the experimental data and generated by using Origin 2019b software as stated previously. The isotherm models are expressed via Eqs. 8, 9, and 10 respectively, were applied to determine the isotherm parameters.

$$q_e = \frac{q_m K_L C_e}{1 + K_L C_e} \tag{8}$$

$$\log q_e = \log K_f + \frac{1}{n}\log C_e \tag{9}$$

$$q_e = \frac{RT}{b_T}\ln k_t + \frac{RT}{b_T}\ln C_e \tag{10}$$

The C_e represents the equilibrium concentration of phenol (mg L^{-1}), q_m is the maximum homogeneous coverage capacity (mg g^{-1}) and K_L is the Langmuir isotherm constant (L mg^{-1}). The values of q_m and K_L can be obtained from the slope and intercept of 1 q_e^{-1} against 1 C_e^{-1} plot, respectively. Whereas K_f is the Freundlich isotherm constant, n is the adsorption intensity constant, and q_e is the amount of adsorbate removed per unit weight of carbon at equilibrium (mg g^{-1}). The value for n and K_f corresponds to the slope and intercept of plot log q_e against log C_e, respectively. On the other hand, from Temkin isotherm, R represents the universal gas constant (8.314 J mol^{-1} K^{-1}), T(K) is the absolute solution temperature, K_t (L g^{-1}) is the equilibrium binding constant which corresponds to the optimum binding energy, and $\frac{RT}{b_T}$ (J mol^{-1}) is the constant related to the heat of sorption. The plot of q_e against l_nC_e will give K_t and $\frac{RT}{b_T}$ from the intercept and slope, respectively.

Table 1
Lignocellulosic composition of raw bamboo (*Dendracalamus asper)*.

Lignocellulosic composition (%)				References
Extractive	Cellulose	Hemicellulose	Lignin	
5.5 ± 0.2	48.3 ± 1.5	17.3 ± 0.4	29.6 ± 0.2	**This study**
5	47.8	19.2	28.4	(Subyakto et al., 2017)
3.9	44.8	18.7	28	(Fatriasari et al., 2014)
N/A	47	16	18	(Kuttiraja et al., 2013)
N/A	41	27	27	(Leenakul and Tippayawong, 2010)
N/A	24.8	22.3	52.9	(Sudibandriyo and Oratmangun, 2018)

*N/A = Not available

2.9. Statistical analysis

The statistical analyses for this study were conducted using Microsoft Excel and Origin 2019b software version 9.6.5. These tools were employed to evaluate and interpret the experimental data systematically. Descriptive statistics, including mean, standard deviation (SD), standard error (SE), residual sum of squares (RSS), and chi-square (χ^2) were calculated to provide a summary of the data distribution. Inferential statistical tests were performed to determine the significant differences among the experimental groups. These tests included Analysis of Variance (ANOVA) where appropriate, to evaluate the statistical significance at a confidence level of 95 % ($p < 0.05$).

3. Results and Discussions

3.1. Characteristics of raw bamboo

The chemical composition of raw bamboo (*Dendrocalamus asper*) is presented in Table 1. The major constituents of bamboo are cellulose (48.3 %), lignin (29.6 %), and hemicellulose (17.3 %). The composition of lignocellulose closely resembled the results reported by other researchers studying *Dendracalamus* sp (Fatriasari et al., 2014; Subyakto et al., 2017). However, Sudibandriyo & Oratmangun (Sudibandriyo and Oratmangun, 2018) reported a different trend in chemical composition, with higher lignin content (52.9 %) and lower cellulose content (24.8 %) in bamboo from the same species. The variation in chemical constituents in bamboo may be due to the geographical location of cultivation, even within the same species (Rini et al., 2023). Changes in chemical constituents in bamboo are influenced by its age; a decrease in cellulose content indicates older bamboo (Li et al., 2010), which might explain the opposite trend observed in the raw bamboo studied (Sun et al., 2011). Research has shown that the holocellulose composition of bamboo is approximately 69.8 %, 68.8 %, and 66.4 % for 1, 3, and 5-year-old bamboo, respectively (Cheng et al., 2015). The bamboo material used in this study is over five years old, as indicated by the 65.6 % holocellulose content. Bamboo maturity varies by species; however, it generally reaches full maturity within 3–4 years, attaining optimal height and biomass suitable for commercial activated carbon production (Kuttiraja et al., 2013). Younger bamboo typically contains higher levels of ash and extractives, which are undesirable for producing high-quality activated carbon. Therefore, mature bamboo is preferred due to its more favourable physicochemical properties (Leenakul and Tippayawong, 2010). Typically, a high holocellulose content in lignocellulosic biomass such as the 65.6 % holocellulose and 29.6 % lignin observed in this study is desirable, as holocellulose decomposes at lower temperatures (200–400°C), promoting the development of pores and enhancing the surface characteristics of the resulting activated carbon (Jablonsky et al., 2013).

The relationship between carbon content and heating values of lignin has a significant linear correlation between these factors was previously observed (Jablonsky et al., 2013). In this study, raw bamboo exhibited a considerably high lignin content (29.6 %) compared to other studies as shown in Table 1, suggesting that it has the potential to yield a high-quality AC with a high carbon composition. It was reported that biomass-rich lignin develops relatively high micropore volumes during pyrolysis (Cagnon et al., 2009).

3.2. Production and characterization of bamboo charcoal

3.2.1. Effect of temperature (°C) and holding time (h) by tube furnace

The carbonization conditions, such as temperature and holding time, are crucial in producing bamboo charcoal (BC) with high porosity. This process increases the carbon content in the precursor and removes non-carbon components through thermal degradation (Pallarés et al., 2018a). Table 2 shows how temperature and holding time impact the yield and properties of BC. The yield of BC decreased significantly from 50.2 % to 26.7 % as the temperature increased from 300 to 700°C due to an accelerated burning rate. This

Table 2
Proximate analysis of bamboo charcoal (BC) produced at various carbonization temperatures and holding times.

Bamboo charcoal	Carbonization conditions	Yield (%)	Proximate analysis (%)			
			Fixed carbon	Volatile matters	Moisture content	Ash
Raw bamboo	N/A	N/A	26.0 ± 3.3	65.5 ± 8.1	6.2 ± 0.5	2.5 ± 1.9
Effect of temperature (°C)						
BC300–2	300	50.2 ± 3.1	57.8 ± 5.9	29.1 ± 8.6	5.5 ± 1.4	2.3 ± 0.1
BC400–2	400	35.8 ± 0.3	67.6 ± 2.1	20.9 ± 6.1	5.1 ± 0.2	4.9 ± 3.9
BC500–2	500	31.9 ± 1.5	78.3 ± 7.3	13.0 ± 2.1	2.4 ± 0.8	4.9 ± 3.2
BC600–2	600	29.3 ± 1.2	72.9 ± 0.5	12.9 ± 1.5	4.0 ± 1.1	8.7 ± 2.0
BC700–2	700	26.7 ± 1.2	65.3 ± 3.1	12.3 ± 0.8	5.1 ± 0.2	14.8 ± 4.3
Effect of holding time (h)						
BC500–1	1	31.1 ± 1.7	68.2 ± 1.5	21.0 ± 4.1	6.8 ± 1.5	2.6 ± 1.5
BC500–2	2	31.9 ± 1.5	78.3 ± 7.3	13.0 ± 2.1	2.4 ± 0.8	4.9 ± 3.2
BC500–3	3	31.5 ± 1.1	69.3 ± 4.5	13.0 ± 2.1	3.8 ± 0.9	11.9 ± 2.5
BC500–4	4	31.2 ± 2.1	69.4 ± 6.8	11.6 ± 3.0	3.6 ± 0.7	13.8 ± 3.6

N/A = Not available

decline is attributed to changes in the lignin and cellulose content of the biomass, along with the conversion of organic matter into ash, leading to an overall reduction carbon content of the BC at a higher temperature (Khater et al., 2024). A similar reduction in biochar yield was observed for mixed wood waste and coconut husk waste biochar as the pyrolysis temperature increased from 400 to 600°C, with yields decreasing from 36.3 % to 24.2 % and 41.4–33.0 %, respectively (Suresh Babu et al., 2024). Similarly, a comparable decline in biochar yield from rice straw and sawdust was reported, which decreased from 378.2 to 216.7 g kg^{-1} and 331.4–204.1 g kg^{-1}, respectively, as the carbonization temperature rose from 400 to 800°C (Khater et al., 2024). Commonly, precursors with a higher fixed carbon content have been found to yield more biochar during the pyrolysis process. This is preferable as it is more economic-friendly, as increased biochar production provides a greater quantity of material for pollutant capture applications (De et al., 2013). In this study, the optimal carbonization conditions for biochar production were determined based on the fixed carbon content, with a higher fixed carbon content being preferred, as discussed in the following sections.

Following the proximate analysis presented in Table 2, it was observed that during the process of carbonization, the fixed carbon content of raw bamboo increased significantly from 26.0 % to 78.3 % within the temperature range of 300–500°C. However, a contrasting trend was noted at temperatures exceeding 500°C, where the fixed carbon content declined to 72.9 % and 65.3 % at 600°C and 700°C, respectively. This reduction at higher temperatures can be attributed to the extensive thermal decomposition or volatilization of organic materials present in the carbonaceous substance, leading to an overall decrease in fixed carbon content (Jagtoyen and Derbyshire, 1998). It was noted that there is a significant reduction in volatile content, from 65.5 % in raw bamboo to 12.3 % at 700°C. This suggests that raw materials with higher volatile matter are more suitable for BC production, as they facilitate easier burning and ignition, leading to improved pore formation during thermal degradation (Phothong et al., 2021). The moisture content decreases as the temperature rises from 300–500°C, dropping from 5.5 % to 2.4 %. However, at 600°C and 700°C, a slight increase in moisture content is observed, reaching 4 % and 5.1 %, respectively. This is likely attributed to the formation of reaction water at elevated temperatures, especially above 500°C, as a byproduct of the thermal decomposition of organic materials. Reaction water can increase the overall moisture content of the resulting pyrolysis products. Studies indicate that higher initial moisture content in the feedstock results in greater production of reaction water, which may further raise the moisture levels in the final products (Demirbas, 2004). Meanwhile, the ash content exhibits an increasing trend, rising from 2.3 % at 300°C to 14.8 % at 700°C. As the pyrolysis temperature increases, there is a saturation of inorganic materials and compounds following the release of organic volatile compounds, leading to an increase in ash content. It is noteworthy that the moisture content and ash content across all samples (BC300–2 to BC700–2) fell within the typical commercial value acceptable range of 5–8 % for moisture content and 2–10 % for ash content except for BC700–2 sample (Dizbay-Onat et al., 2018; Jabit, 2007). Consequently, a carbonization temperature of 500°C is considered the optimal temperature, yielding the highest fixed carbon content of 78.3 %.

The study also examined how different holding times affected the yield and texture of BC, and the results also presented in Table 2. Increasing the holding time from 1 to 2 h led to a rise in fixed carbon content from 68.2 % to 78.3 %. However, extending the carbonization process beyond 2 h caused the fixed carbon content to drop. This was attributed to the increased consumption of carbon atoms, consequently causing the collapse of the carbon structure and pore wall (Lua, 2024). Consequently, there was a decline in fixed carbon content beyond 2 h of carbonization holding time. The breakdown of carbon atoms also resulted in higher ash formation, evidenced by the increase of 11.9 % and 13.8 % ash content at 3 h and 4 h of carbonization, respectively as compared to BC500–2 (4.9 %). Based on the proximate analysis of the BC, the optimal carbonization conditions were determined to be 500°C for 2 h (BC500–2). Under these conditions, the BC produced exhibited a yield $>$ 30 %, with high fixed carbon content (78.3 %), low moisture content (2.4 %) and low ash content (4.9 %) before activation conditions optimization step.

3.3. Production and characterization of bamboo activated carbon

3.3.1. Effect of temperature (°C) and holding time (h) by tube furnace

The activation of BC to produce BAC was conducted using a tube furnace under ranges of activation temperatures and holding times (Table 3). The yield of BAC700–2 and BAC800–2 was recorded at 28.2 % and 19.8 % respectively, in comparison to BAC900–2 and BAC1000–2 ($<$10 %). The low yield of BAC is a major drawback, as it results in a smaller final product obtained from the same amount of starting material. Consequently, this is considered economically inefficient and leads to an increase in the production costs per unit

Table 3
Yield and textural properties of bamboo activated carbon (BAC) produced at various activation temperatures and holding time.

BAC	Yield (%)	SSA (m^2 g^{-1})	V_T (cm^3 g^{-1})	V_μ (cm^3 g^{-1})	V_u/V_T (%)	V_M (cm^3 g^{-1})	d_p (nm)
Effect of temperature (°C)							
BAC700–2	28.2 ± 1.1	540.7	0.24	0.22	93.2	0.016	1.75
BAC800–2	19.83 ± 0.9	1336.1	0.56	0.54	96.0	0.022	1.68
BAC900–2	8.29 ± 7.1	965.8	0.40	0.39	97.1	0.012	1.66
BAC1000–2	2.10 ± 1.8	502.8	0.23	0.21	92.3	0.017	1.81
Effect of holding time (h)							
BAC800–1	27.83 ± 1.2	550.7	0.28	0.27	95.9	0.011	2.04
BAC800–2	19.83 ± 0.9	1336.1	0.56	0.54	96.0	0.022	1.68
BAC800–3	20.31 ± 0.5	1061.3	0.44	0.41	93.2	0.030	1.66
BAC800–4	8.65	1041.1	0.53	0.52	97.6	0.013	2.05

of BAC (León et al., 2020). An activation temperature above 900°C is undesirable for producing BAC. The surface area of BAC gradually increased as the temperature rose from 700°C to 900°C, however, the surface area reduced to 502.8 $m^2\ g^{-1}$ at an elevated activation temperature of 1000°C. This circumstance arises as pores on the carbon materials rupture at elevated temperatures, diminishing the surface of the BAC (Hock and Zaini, 2018). A similar trend of porosity reduction at an elevated temperature, attributed to the merging of pores (Phothong et al., 2021).

In hindsight, the BAC produced in the lab-scale study was highly microporous, with micropore percentages exceeding 90 % for all sample sets from BAC700–2 to BAC1000–2. Micropores have a diameter of less than 2 nm, mesopores range from 2 nm to 50 nm, and macropores have a diameter greater than 50 nm (Thommes et al., 2015). This is further confirmed by the pore size of all samples (1.66–1.81 nm), which remained below 2 nm as shown in Table 3. Therefore, an activation temperature of 800°C with a surface area of 1336.1 $m^2\ g^{-1}$ was considered appropriate for producing high-porosity BAC before holding time condition optimization was conducted.

Subsequently, the impact of varying holding times on BAC yield and textural properties was examined (Table 3). Prolonged activation periods exceeding 2 h result in a higher release of volatiles, leading to a reduction in the surface area and porosity of BAC, as demonstrated by BAC800–3 (1061 $m^2\ g^{-1}$) and BAC800–4 (1041 $m^2\ g^{-1}$). A high surface area is a crucial characteristic of BAC, as it provides more sites for molecules to adhere to the carbon surface. This, in turn, increases the overall adsorption capacity of the AC, enabling it to capture and retain a larger quantity of contaminants or target substances (Liang et al., 2020). The BAC produced at different holding times was predominantly microporous, with micropore percentages exceeding 90 % across all samples. According to Sánchez-Díaz et al. (2022), micropores in activated carbon are essential for enhancing the diffusion of phenol molecules, which improves adsorption capacity.

Another finding reported that increasing the activation temperature led to an expansion in micropore width, thereby increasing phenol uptake from 164 to 217 mg g^{-1} , highlighting the critical role of microporosity in pollutant adsorption (Hock and Zaini, 2018). Based on the analyzed textural properties, the optimal conditions for BAC production were identified as thermal decomposition at 500°C for 2 h, followed by activation at 800°C for 2 h, achieving the highest specific surface area in the lab-scale study. These optimized conditions were subsequently applied in the two-in-one reactor (pilot-scale study) to assess the characteristics and properties of the resulting BAC, as well as its performance in phenol removal applications.

3.3.2. Effect of size on BAC production using two-in-one carbonization activation reactor

Table 4 presents the yield and textural properties of BAC produced by pilot-scale study at different sample sizes. Among the tested samples of different sizes, the 5 × 2 cm BAC exhibited the highest surface area (1018.4 $m^2\ g^{-1}$), along with significant microporosity (>85 %) and a pore diameter of 2.08 nm. These features indicate the effective development of porous structures, achieved within a relatively short 4-hour process in comparison to the previous study by using oil palm kernel shell as raw material, which took about 7 h to obtain activated carbon with surface area of 935 $m^2\ g^{-1}$ (Nahrul Hayawin et al., 2018).

Interestingly, the specific surface area of the BAC showed a size-dependent trend. The largest sample size demonstrated the highest surface area (1018.4 $m^2\ g^{-1}$), whereas the smallest sample size exhibited the lowest (482.7 $m^2\ g^{-1}$). This variation can be attributed to the sample arrangement during activation. Smaller samples are more likely to stack, which disrupts uniform exposure to the activating agent across the sample surfaces. This uneven contact, particularly for samples positioned at the bottom, reduces gas-solid interactions and thus lowers the specific surface area. In contrast, larger, non-stacked samples facilitate greater direct exposure to steam enhancing the activation process and resulting in higher surface areas.

Steam activation is known for its higher reactivity at elevated temperatures, which promotes the widening of micropores and the formation of mesopores. As a result, the BAC produced exhibited a comparatively lower micropore percentage (<90%) as notably observed in 5 × 2 cm sample size. Molina-Sabio et al. (1996) reported similar findings, where steam activation primarily enlarged existing micropores rather than creating new ones, influencing both surface area and pore size distribution. Likewise, Pallarés et al. (2018b) found that steam activation tends to reduce microporosity and encourage mesopore development, making the material suitable for adsorbing a wider range of pollutant sizes. This broader pore size distribution enhances the versatility of BAC, especially for applications involving larger molecules or requiring rapid adsorption kinetics (Zhou et al., 2021).

The BAC sample produced using the two-in-one reactor with a size of 5 × 2 cm exhibited the highest surface area (1018.4 $m^2\ g^{-1}$) and was identified as the optimal sample. Therefore, BAC800–2 with a 5 × 2 cm size was selected for further evaluation of its efficiency in phenol removal. On the other hand, the BAC samples from the tube furnace were not utilized for the phenol removal study, as they were part of a preliminary investigation aimed at determining the optimal carbonization and activation conditions for producing BAC from two-in-one reactor.

Table 4
Textural properties of bamboo activated carbon (BAC800-2) produced at different sample sizes.

Reactor	Sample size (cm)	Yield (%)	SSA ($m^2\ g^{-1}$)	V_T ($cm^3\ g^{-1}$)	V_μ ($cm^3\ g^{-1}$)	V_u/V_T (%)	V_M ($cm^3\ g^{-1}$)	d_p (nm)
Two-in-one reactor	1 × 1	19.3 ± 1.2	482.7	0.20	0.17	85.00	0.03	1.64
	5 × 2	18.9 ± 2.5	1018.4	0.53	0.46	87.03	0.07	2.08

3.4. Batch adsorption study of phenol removal

3.4.1. Effect of dosage and contact time

The determination of phenol removal efficacy at different sorption parameters is crucial for achieving optimal phenol binding to BAC. Three sorption parameters were investigated: contact time, adsorbent dosage and pH. The point of optimal phenol removal was identified at adsorption equilibrium. Fig. 1 illustrates the percentage of phenol removal at various BAC800–2 dosages ranging from 0.1 g to 0.5 g (corresponding to concentrations of 2 g L^{-1} to 10 g L^{-1}), agitated for 210 min. As the adsorbent dosage increased, there was a gradual rise in phenol uptake: 64 % (0.1 g) and reaching to 99 % (0.5 g) at a maximum contact time of 210 min. This trend can be attributed to the higher active sites and pores provided by BAC800–2 at a higher dosage (0.5 g) in comparison to the lower dosage (0.1 g), resulting in a noticeable difference in phenol uptake. This is because a higher concentration of adsorbents provides an abundance of active sites and pores, leading to an increased affinity of contaminants towards AC (Kumar Shetty et al., 2022).

The initial 15 min of adsorption revealed rapid phenol uptake across varying dosages of BAC800–2 adsorbent, indicating active adsorption onto its pores. Notably, higher dosages (0.3 g to 0.5 g) exhibited substantial adsorption rates of 87.8 %, 94.1 %, and 97.4 % respectively within this brief timeframe. Beyond this period, phenol uptake reached equilibrium around 30 min (Fig. 1), suggesting saturation of adsorption sites within BAC800–2. This observation aligns with the findings of Tan et al. (2021) who noted that adsorption capacity is limited by available sites once equilibrium is achieved, regardless of extended mixing times. In contrast, lower adsorbent dosages displayed a gradual increase in phenol removal over time, with equilibrium times noted at approximately 120 min and 90 min respectively for dosages of 0.1 g and 0.2 g. This delay is attributed to fewer active sites and pores, resulting in a higher adsorbate-to-adsorbent ratio and necessitating an extended contact period for complete phenol saturation (Djelloul et al., 2017; Sazali et al., 2020). This can be attributed to the presence of fewer available active sites and pores, thus reducing the initial contact between phenol and BAC800–2 owing to a higher ratio of adsorbate to adsorbent. Consequently, it takes a longer time for all pores to be fully saturated with phenol, requiring an extended contact period to achieve equilibrium (Djelloul et al., 2017; Sazali et al., 2020).

Conversely, the adsorption capacity exhibits a declining trend as the adsorbent dosage increases. At a dosage of 0.1 g, the adsorption capacity reaches its maximum value of approximately 30 mg g^{-1} , as illustrated in Fig. 2. However, with an increase in dosage to 0.5 g, the adsorption capacity steadily decreases to around 10 mg g^{-1} .

This reduction in adsorption capacity with higher adsorbent dosages is attributed to the incomplete utilization of active sites. At lower dosages, the active sites on the adsorbent are fully occupied, leading to a higher adsorption capacity. In contrast, at higher dosages, the available phenol is distributed across more adsorbent particles, leaving many active sites unutilized (Ho, 2022; Gabr et al., 2023; Neziri and Duranoğlu, 2024). As a result, the adsorption capacity (per gram of BAC) decreases. To summarize, although increasing the adsorbent dosage improves phenol removal efficiency, it reduces the adsorption capacity. This behaviour is commonly observed in adsorption studies, where higher dosages enhance removal efficiency but result in underutilization of the adsorbent surface. Table 5 provides a comparative analysis of phenolic compound removal using activated carbon derived from various raw materials. Additionally, a comparative study was conducted by applying a selected set of experimental conditions to commercial bamboo activated carbon, as detailed in Table 5. The findings revealed that BAC800–2 exhibited significantly higher phenol adsorption efficiency, achieving 98.5 % removal compared to 82.4 % for commercial bamboo activated carbon under the same treatment conditions. This demonstrates that BAC800–2 is 1.19 times more effective in phenol removal, emphasizing its superior adsorption performance.

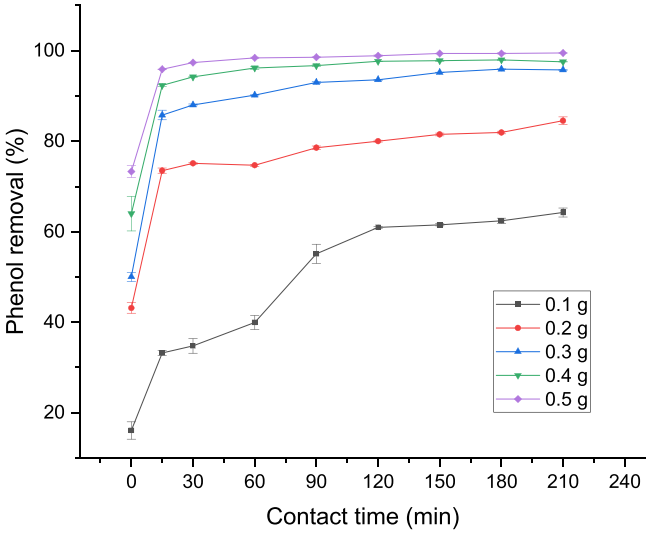

Fig. 1. Phenol removal efficiency (%) of BAC800–2 at varying dosages (0.1–0.5 g) under agitation at 180 rpm for 210 min at 25 °C. The experiment was conducted with an initial phenol concentration of 100 mg L^{-1} at a fixed pH of 7. Error bars represent the standard deviation of the mean (n = 3).

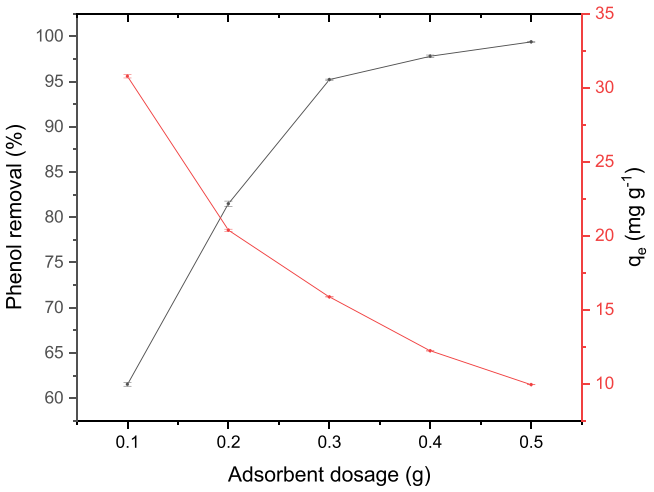

Fig. 2. The impact of increasing adsorbent dosage (g) on adsorption capacity (mg g^{-1}) and phenol removal efficiency (%). Error bars represent the standard deviation of the mean (n = 3).

Table 5
Comparison of phenolic compounds removal by activated carbon (AC) produced from various types of raw material.

Raw material	Preparation method	Adsorption condition	Phenol removal (%)	Adsorption capacity	References
Bamboo	Physical activation	Agitated at 180 rpm at 25°C for 60 min	98.5	24.05 mg g^{-1} at 100 mg L^{-1} of phenol initial concentration	This study
Bamboo (Commercial BAC)	N/A	Agitated at 180 rpm at 25°C for 60 min	82.4	8.24 mg g^{-1} at 100 mg L^{-1} of phenol initial concentration	This study
Banana peels	Chemical activation	Agitated at 150 rpm at 30°C for 120 min	83	6.98 mg g^{-1} at 50 mg L^{-1} of phenol initial concentration	(Ingole et al., 2017)
			60	48.58 mg g^{-1} at 500 mg L^{-1} of phenol initial concentration	
Tomato stem	Chemical activation	Agitated at 150 rpm at 35°C for 120 min	92	32.76 mg g^{-1} at 30 mg L^{-1} of phenol initial concentration	(Dasgupta et al., 2016)
Purchased GAC	N/A	Continuous column at 21°C	N/A	32.4 mg g^{-1} at 50 mg L^{-1} of phenol initial concentration	(AL-Doury and Alwan, 2021)
Sawdust	Chemical activation	Agitated at 120 rpm at 25°C for 350 min	87	2.82 mg g^{-1} at 100 mg L^{-1} of phenol initial concentration	(Mohanty et al., 2005)
Water hyacinth	Chemical activation	Agitated at 400 rpm at 30°C for 4 h	94	0.47 mmol g^{-1} at 1 mmol L^{-1} of initial phenol concentration	(Varghese et al., 2004)

*N/A = Not available

3.4.2. *Effect of pH*

Wastewater consists of various constituents, including suspended solids, organic and inorganic pollutants, pathogens, heavy metals, and toxic compounds. Among these, phenol is categorized as a persistent organic pollutant due to its resistance to degradation and harmful environmental effects (Varghese et al., 2004). The pH of real-life wastewater can vary widely, depending on the nature of the industrial activities and wastewater sources. Real wastewater samples have been reported with pH values ranging from as low as 2.5 to as high as 12.9; however, typical values generally fall between pH 6 and 8 (Kilic et al., 2011; Taraba and Bulavová, 2018; Xie et al., 2020). In Malaysia, the Department of Environment (DOE) specifies acceptable effluent discharge standards within the pH range of 5.5–9 (Department of Environment, 2020).

To evaluate the robustness of the adsorbent under various conditions, a broad pH range of 2–12 was investigated in this study. The pH of the solution significantly influences the efficacy of phenol removal, as it directly affects the speciation of phenol and the surface charge characteristics of AC. Lower pH conditions generally favour the adsorption of negatively charged species due to the abundance of H^+ ions, whereas higher pH levels support the adsorption of positively charged species due to the presence of OH^- ions (Lu et al., 2011). This study examined the impact of pH on phenol removal efficiency across a range from pH 2–12, as illustrated in Fig. 3.

The results demonstrate that phenol removal efficiency increases from 97 % to 99 % as the pH rises from 2 to 8. Beyond pH 8, a gradual decline in removal efficiency is observed, reaching 95 %, followed by a significant drop to 77 % at pH 12. Phenol, with a pKa of 10, predominantly exists in its neutral molecular form below pH 10 (Taraba and Bulavová, 2018). Under these acidic to neutral conditions, the rapid adsorption of phenol onto BAC800–2 is facilitated by its extensive surface area and the numerous active sites available for effective phenol entrapment.

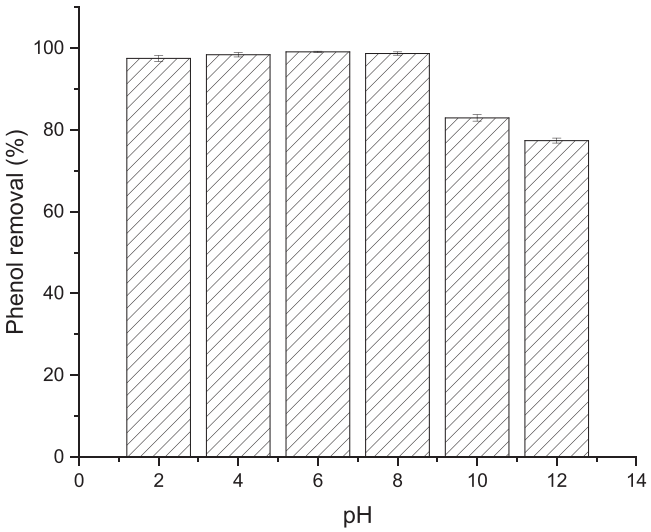

Fig. 3. The influence of pH (ranging from 2–12) on the adsorption efficiency of phenol onto the surface of BAC800–2 under agitation at 180 rpm for 60 min at 25°C. The experiment was conducted with an initial phenol concentration of 100 mg L^{-1} , maintained at a fixed pH of 7. Error bars represent the standard deviation of the mean (n = 3).

At pH values above 8, the surface charge of BAC800–2 transitions from positive to negative as the pH surpasses the point of zero charge (pH_{pzc} = 7.42) as shown in Fig. 4. This shift results in decreased phenol uptake, as phenol molecules begin to compete with H^+ ions for adsorption sites due to the electrostatic interactions with water molecules in the system. This phenomenon has been reported, where competitive adsorption between water molecules and phenol was observed, leading to a reduction in phenol adsorption capacity (Xie et al., 2020). At pH levels above 10, the phenol removal efficiency sharply declines to 77.4 %. This decrease is attributed to the electrostatic repulsion between the negatively charged surface of BAC800–2 and the $C_6H_5O^-$ anions formed as phenol ionizes in highly alkaline conditions (Lu et al., 2011). This repulsion significantly reduces adsorption efficacy, highlighting the need to maintain optimal pH levels for effective phenol removal.

3.5. Kinetic study

Understanding the kinetics of adsorption is essential for elucidating the dynamics of the process, including diffusion control and mass transfer of the phenol into the BAC (Saleh, 2022). In this study, four kinetic models were employed to analyze the experimental data: PFO, PSO, Elovich, and IPD models, as illustrated in Fig. 5. The calculated kinetic parameters for each kinetic model are summarized in Table 6. Typically, correlation coefficient (R^2) value is evaluated to determine the best kinetic model in describing the adsorption process and mechanism (Surela et al., 2024). Both PFO and PSO result in a very high and close R^2 value of 0.9995 and 0.9945 respectively with only a 0.005 (9 %) difference. Elovich model gives slightly lower R^2 at 0.9720 follows by the lowest R^2 value

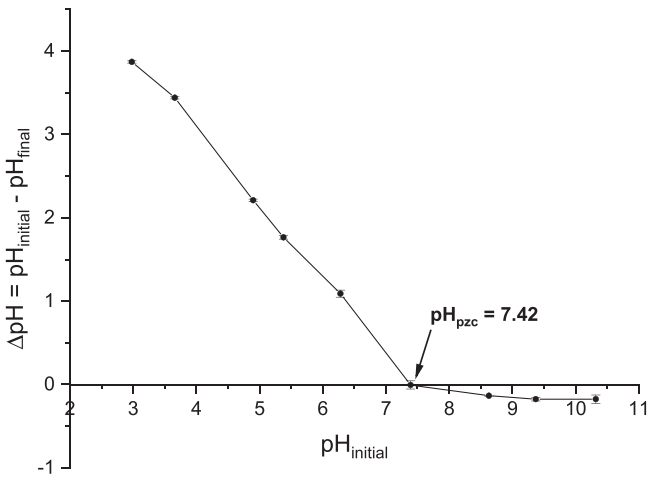

Fig. 4. Point of zero charge (pH_{pzc}) determination for BAC800–2. Error bars represent the standard deviation of the mean (n = 3).

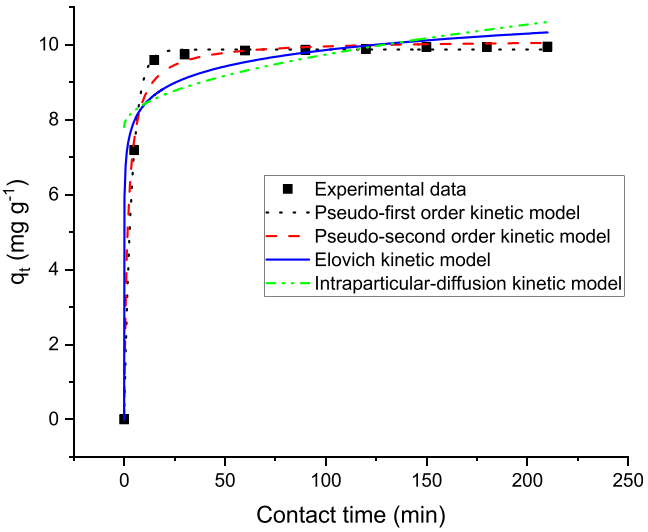

Fig. 5. Kinetic study of phenol adsorption onto the BAC800–2 by 4 different models.

Table 6
The kinetic parameters of pseudo-first-order (PFO), pseudo-second-order (PSO), Elovich, and intraparticle diffusion (IPD) models for the phenol adsorption onto bamboo activated carbon (BAC800-2).

Kinetic models	Parameters	
PFO	k_1 (min^{-1})	0.2589
	R^2	0.9995
	χ^2	0.0049
	RSS	0.0391
PSO	k_2 (g (mg min)$^{-1}$)	0.0552
	R^2	0.9945
	χ^2	0.0543
	RSS	0.4345
Elovich	α ((mg g^{-1}) min)	1.75×10^5
	β (g mg^{-1})	1.7496
	R^2	0.9720
	χ^2	0.2748
	RSS	2.1987
IPD	k_3 (mg (g min)$^{-0.5}$)	0.4389
	C (mg g^{-1})	5.0852
	R^2	0.4169
	χ^2	5.7302
	RSS	45.8412

represents by IPD model. Due to the very slight difference of correlation coefficient (R^2) reported, particularly by PFO and PSO models, other parameters such as chi-square (χ^2) and, adsorption capacity (q_e) and adsorption rate constant (min^{-1}) need to be considered to determine the best kinetic model to describe the adsorption process. The chi-square value represents a quantitative measurement of the difference between the experimental and expected (model) values. Smaller chi-square value gives a better fit, indicating that the model closely obeys the experimental data. The chi-square function (χ^2), shown in Eq. 11, compares the experimental value of adsorption capacity (q_{exp}, mg g^{-1}) with the theoretically expected value of adsorption capacity (q_{cal}, mg g^{-1}) from the fit model (Afkhami et al., 2010; Naiya et al., 2009).

$$\chi^2 = \sum \frac{\left(q_{\exp} - q_{cal}\right)2}{q_{cal^2}} \tag{11}$$

PFO model has smaller χ^2 value of 0.0049 and compared to PSO model of 0.0543, suggesting that PFO model fits the experimental the best. Further supporting the PFO as the best fit model, is by comparing the expected adsorption capacity (q_{cal}) for the PFO model (9.87 mg g^{-1}) with experimental, q_{exp} (9.74 mg g^{-1}), which is very close in value. However, the PSO model's expected adsorption capacity q_{cal} (10.13 mg g^{-1}) is slightly higher than the experimental q_{exp} (9.74 mg g^{-1}) indicating the adsorption of phenol onto BAC800–2 obeys PFO model the best. Additionally, as stated in Table 6, the residual sum of squares (RSS) for the PFO model is the lowest (0.0391) compared to the PSO model (0.4345), indicating a better fit. A lower RSS value signifies a model with higher accuracy

in describing the experimental data.

Moreover, the adsorption rate constants (min^{-1}) between PFO (k_1) and PSO (k_2) could be taken into account in determining the best fit model of kinetic study. The results exhibit a significant disparity between the PFO and PSO models. The PFO model demonstrates a much faster adsorption process for phenol, with a rate constant k_1 of 0.2589 min^{-1} , while the PSO model shows a slower rate constant k_2 of 0.0552 min^{-1} . The adsorption rate of phenol onto the surface of BAC800–2 by the PFO model is 4.69 times higher than that of the PSO model. Taking into consideration all the parameters discussed, it can be deduced that the adsorption process of phenol onto the BAC surface obeys the PFO model the best. In the PFO model, adsorption process control is primarily governed by the adsorbate concentration, within a homogenous system. The occupation of adsorbate on the surface of adsorbent mainly through physical adsorption which drives rapid initial diffusion by van der Waals forces (Mashhadimoslem et al., 2024; Plazinski and Rudzinski, 2009; Rudzinski and Plazinski, 2006). The PSO model's assumptions are reflected in phenol removal by BAC800–2 as a very swift initial diffusion (external and internal) was observed at a higher adsorbent dosage of 0.4 g and 0.5 g, achieving 94.1 % and 97.4 % just within the first 15 min. The adsorption process reaches equilibrium in about 30 min at a higher dosage indicating that most of the surface of BAC800–2 has been occupied by phenol in a homogenous manner. Therefore, considering all the kinetic parameters, it is concluded that the PFO model best fits the adsorption kinetics.

The adsorption rate and mechanism of phenol onto the BAC surface were analyzed using the intraparticle diffusion (IPD) model. This model describes the adsorption process as involving three sequential steps: (I) external diffusion of the adsorbate through the boundary layer to the adsorbent surface, (II) pore or intraparticle diffusion within the adsorbent, and (III) adsorption of the adsorbate onto active sites on the surface (Fathiganjehlou et al., 2024; Hu et al., 2024). To evaluate the significance of these steps, a linear fit of the intraparticle diffusion model was applied. A linear plot passing through the origin indicates that the adsorption process is governed solely by intraparticle diffusion, controlled by internal diffusion. Fig. 6 presents the relationship between the amount of phenol adsorbed (q_t, mg g^{-1}) against $t^{0.5}$ ($min^{0.5}$) for BAC800–2.

As illustrated in Fig. 6, the concentration profile reveals three distinct steps during the adsorption process. The first step (I) represents the rapid diffusion of phenol through the boundary layer to the external surface of the BAC, occurring within the initial 4 min. The second step (II), associated with intraparticle diffusion, displays a more gradual slope, signifying the steady adsorption of phenol into the BAC pores over the 4–8-min interval. Finally, the third step (III) reflects the near attainment of equilibrium, where the rate of intraparticle diffusion slows significantly due to the minimal concentration of phenol remaining in the solution. At this point, linear equilibrium is achieved as the phenol concentration in the solution decreases significantly, leading to complete removal (Adewuyi et al., 2015; Ferreiro et al., 2021).

Fig. 6 clearly demonstrates that the intraparticle diffusion model does not entirely capture the adsorption process, as linearity is not observed across all stages. Notably, the lines corresponding to the second and third stages deviate from the origin, suggesting that while intraparticle diffusion plays a role in the overall adsorption, it is not the predominant mechanism (Hu et al., 2024; Csavdari, 2023). This observation indicates that the adsorption kinetics are governed by mechanisms beyond intraparticle diffusion (IPD). This conclusion is further supported by the relatively low R^2 value of 0.4169 for the IPD model, compared to the higher R^2 values obtained for other kinetic models, as shown in Table 6.

3.6. Isotherm study

The equilibrium isotherms between adsorbent and the adsorbate are essential in describing the type of interaction or mechanism occurring in the adsorption system (Adeleke et al., 2024). In this study, the adsorption of phenol onto BAC800–2 was evaluated using three isotherm models: Langmuir, Freundlich and Temkin as illustrated in Fig. 7. Among these models, the Freundlich isotherm

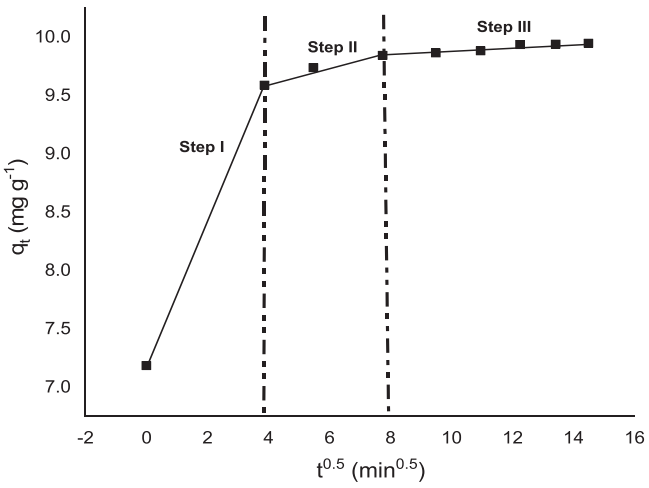

Fig. 6. Linear graph of intraparticle diffusion model for adsorption of phenol by BAC800–2.

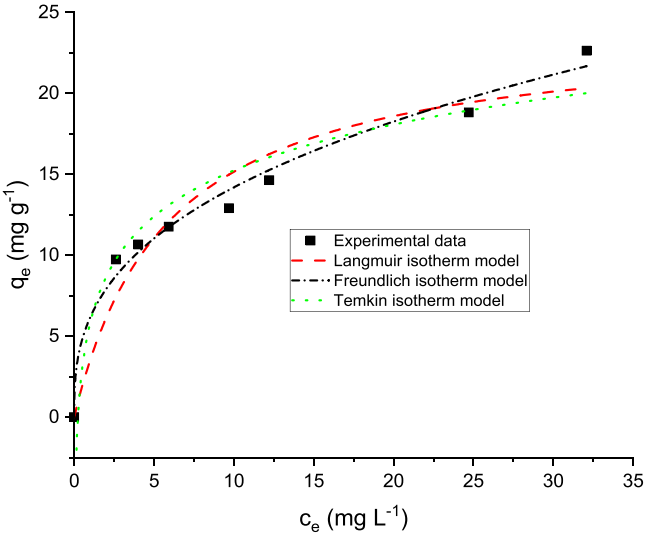

Fig. 7. Presents the isotherm study of phenol uptake by BAC800–2, evaluated using three different models.

provided the best fit, with a coefficient of determination (R^2) of 0.9588 as well as the smallest chi-square function (χ^2) of 0.9119, in comparison to other models as shown in Table 7. This model describes adsorption as a multilayer process occurring on heterogeneous surfaces, where the heat of adsorption and surface affinities vary non-uniformly (Sparks et al., 2024).

For phenol adsorption onto BAC, the Freundlich isotherm indicates a complex physicochemical process. The adsorbate is transferred from the solution phase to the porous interior surface of the BAC, where adsorption occurs (Sparks et al., 2024; Van der Bruggen, 2014). Upon reaching thermodynamic equilibrium between the adsorbate concentration in the solution and on the adsorbent, no further adsorption is theoretically expected (Gök et al., 2008; Srivastava et al., 2006). Due to the Freundlich model's multilayer adsorption, phenol continues to adhere to the BAC surface post-equilibrium at a slower rate. This indicates a complex adsorption process, with phenol forming multiple layers and extending beyond initial equilibrium

3.7. Characteristics of raw bamboo, BC and BAC

3.7.1. Morphological properties using SEM

The surface morphology of raw bamboo, BC500–2, and BAC800–2 was analyzed using scanning electron microscope (SEM). Fig. 8 (a) shows that raw bamboo exhibits a relatively smooth surface with minimal porosity. Following carbonization in the two-in-one reactor, Fig. 8(b) illustrates significant pore development in BC500–2. This transformation occurs as the decomposition of organic material and the release of volatile compounds create pores, thereby increasing the carbon material's porosity. The diverse pore sizes observed are attributed to bamboo's high lignin content, which results in a varied pore size distribution (Rennhofer et al., 2021). During activation, as shown in Fig. 8(c), these pores enlarge further. The varying intensity of steam exposure during activation leads to a range of pore sizes: larger pores emerge from prolonged interaction with steam molecules, while smaller ones result from less consistent contact. The SEM images of BAC800–2 reveal pores distributed across its surface, enhancing its potential for phenol adsorption from multiple angles. Additionally, bamboo's intrinsic porous structure, combined with surface features like slits, enhances

Table 7
Isotherm parameters of Langmuir, Freundlich and Temkin models for the phenol adsorption onto bamboo activated carbon (BAC800-2).

Isotherm model	Parameters	
Langmuir	q_m (mg g^{-1})	24.0369
	K_L (L mg^{-1})	0.1706
	R^2	0.9297
	χ^2	3.1639
Freundlich	K_f (mg g^{-1})	6.14736
	n	2.75219
	R^2	0.9588
	χ^2	0.9119
Temkin	$\frac{RT}{bT}$ (J mol^{-1})	4.0966
	A_T	4.1223
	R^2	0.9429
	χ^2	1.4277

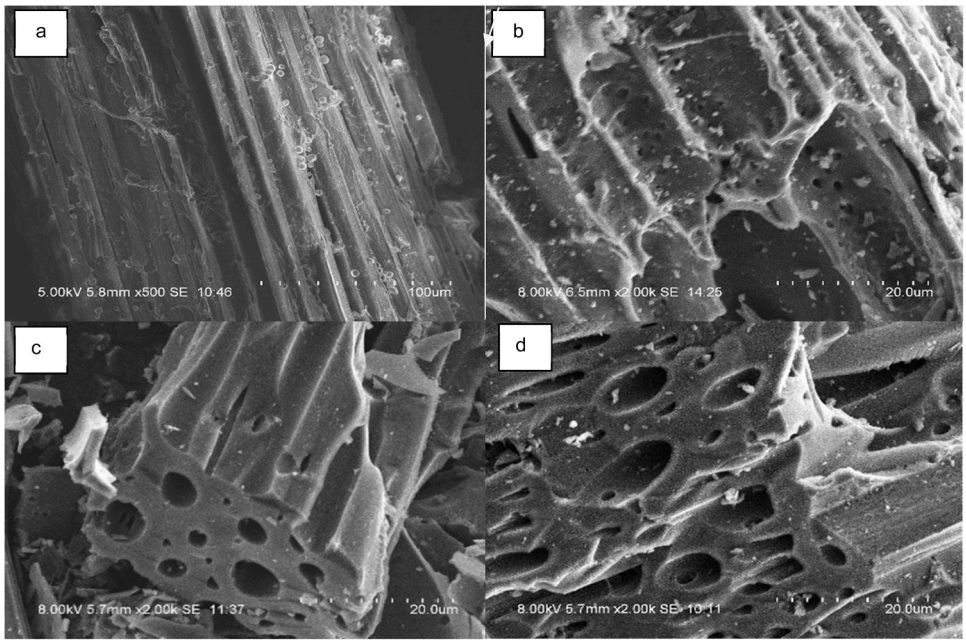

Fig. 8. Morphology of (a) raw bamboo, (b) BC500–2, (c) BAC800–2 and (d) BAC800–2 post-phenol adsorption at 500 and 2.00k magnification.

phenol capture beyond mere pore adsorption.

3.7.2. Elemental properties using EDX

The elemental composition properties of raw bamboo BC and BAC were studied using energy dispersive X-ray (EDX) analysis as displayed in Fig. 9 whereas the percentage of each element is depicted in Table 8. During carbonization, the carbon content of raw bamboo increases from 60 % to 84 %, driven by the expulsion of volatile components, resulting in a carbon-rich BC. Post-activation, however, the carbon content slightly decreases to 79 %. This reduction is due to the exposure of BC to high temperatures during the activation process, leading to further decomposition and a lower carbon yield (Lua, 2024). Raw bamboo's oxygen content starts at 38 % due to moisture and volatile substances, dropping to 10 % after carbonization removes these volatiles.

During the activation process, the oxygen content rises to 16 % in BAC800–2. This increase is attributed to the introduction of oxygen via the steam (H_2O) used as the activating agent in the two-in-one reactor. The presence of trace elements such as magnesium (Mg), sulphur (S), potassium (K), calcium (Ca), and phosphorus (P) increases after both carbonization and activation processes, as seen in Fig. 9. The concentration rises because the overall mass decreases during processing, increasing the relative content of these elements in the final BAC. Specific activation methods, like steam activation, can further introduce or concentrate these trace elements in the BAC (Khuong et al., 2021).

3.7.3. Functional group analysis using FTIR

Fourier transform infrared spectroscopy (FTIR) was employed to analyze the functional groups present in raw bamboo, BC500–2, and BAC800–2, as illustrated in Fig. 10. All samples exhibit a prominent band between 745 and 874 cm^{-1}, indicating strong C-H bonding. This band is more pronounced in BC500–2 and BAC800–2 compared to raw bamboo, suggesting a concentration of carbon content post-carbonization and activation. Strong absorptions around 1239 and 1728 cm^{-1}, in raw bamboo are attributed to C-O stretching in secondary alcohol groups and C═O stretching in amide groups (Lütke et al., 2019; Sun et al., 2019). However, these peaks diminish in BC500–2 and BAC800–2, suggesting the vaporization of organic matter during carbonization and activation, leading to the formation of intrinsic pores (El-Bery et al., 2022). The presence of peak at 2989 cm^{-1} indicates the C–H stretching of methyl and methylene groups from cellulose, hemicellulose, and lignin. The persistence of these peaks suggests these functional groups are retained even after activation and adsorption processes (Fathiganjehlou et al., 2024).

The intense O–H stretching band around 3339 cm^{-1} observed in raw bamboo primarily attributed to adsorbed moisture and surface hydroxyl groups which diminished noticeably in both BC500–2 and BAC800–2, confirming the effective removal of water during pyrolysis (El-Gawad et al., 2025). Following phenol adsorption, a further reduction in the broad O–H stretching band at approximately 3339 cm^{-1} was observed in BAC800–2, indicating the participation of surface hydroxyl groups in hydrogen bonding interactions with phenol molecules. A similar observation was observed by El-Gawad et al. (2025) where the hydroxyl group in phenol results in a O-H stretching vibration, exhibited attenuation after adsorption at 3213 cm^{-1}. This band suggests hydrogen bonding between phenol molecules and their acid activated eggshell derived activated carbon surface area. Besides, a noticeable decrease in intensity of the C–O and C-O-C stretching band at 1109 cm^{-1} suggesting the possibility of hydrogen bonding and π–π interaction (Jibril et al., 2007).

Additionally, the C═O stretching vibration near 1691 cm^{-1} exhibits a slight shift and attenuation post-adsorption, suggesting

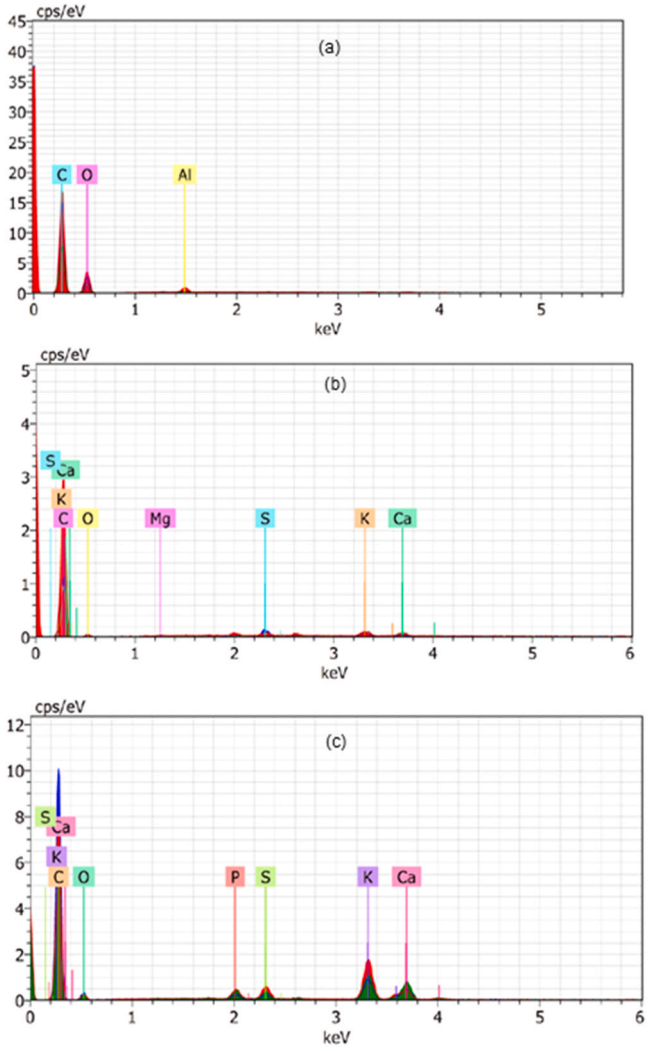

Fig. 9. Elemental composition of (a) raw bamboo (b) BC500–2 (c) BAC800–2 by EDX analysis.

Table 8
Percentage of elemental composition using EDX analysis of raw bamboo, bamboo charcoal (BC500-2) and bamboo activated carbon (BAC800-2).

Sample	Elemental composition (%)							
	C	O	Al	Mg	S	K	Ca	P
Raw bamboo	60.49	38.5	0.63	N/A	N/A	N/A	N/A	N/A
BC500–2	84.69	10.77	N/A	0.63	1.17	1.62	1.27	N/A
BC800–2	79.99	16.4	N/A	N/A	0.94	4.29	2.74	0.94

*N/A = Not available

potential π–π electron donor–acceptor interactions or dipole–dipole interactions between the carbonyl functionalities of BAC and the aromatic ring of phenol (Chen et al., 2025). Subtle broadening and shifts in the C=C stretching bands at 1572 and 1421 cm^{-1} further confirm the presence of π–π stacking interactions between phenol's aromatic structure and the graphitic domains of BAC800–2. On the other hand, the reduced intensity observed in the 869–753 cm^{-1} region after phenol adsorption onto BAC800–2 may indicate the involvement of surface oxygen-containing functional groups such as hydroxyl, carboxyl, or ether groups in forming hydrogen bonds with the phenolic –OH moiety. This observation supports the occurrence of physisorption and is consistent with the findings of El-Gawad et al. (2025), who reported a similar decrease in the 871–751 cm^{-1} band, attributed to hydrogen bonding interactions between surface calcium ions and phenol's hydroxyl group.

In summary, the FTIR analysis confirms that phenol adsorption onto BAC800–2 primarily occurs through physisorption mechanisms. The spectral changes indicate the involvement of multiple non-covalent interactions, including hydrogen bonding, π–π stacking,

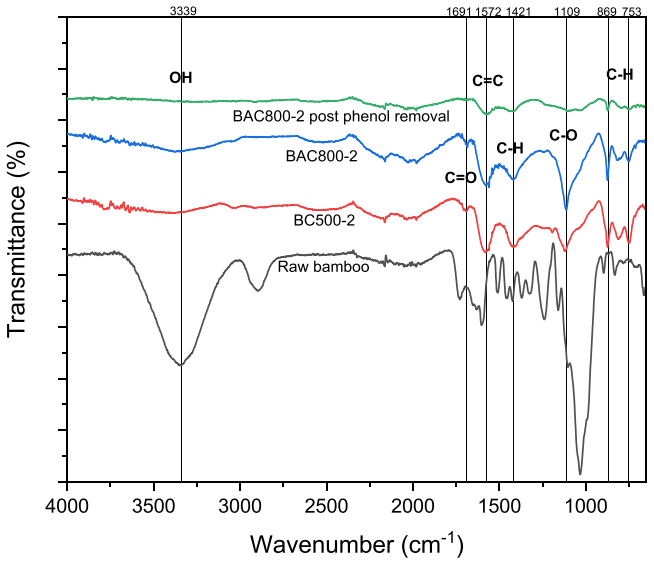

Fig. 10. FTIR spectra of raw bamboo, BC500–2, BAC800–2 and BAC800–2 post phenol adsorption.

π–π electron donor–acceptor interactions, dipole–dipole interactions between phenol and surface oxygenated functional groups. These observations align well with the kinetic and equilibrium modeling results, where the adsorption process follows the pseudo-first-order (PFO) kinetic model, suggesting a physisorption-dominated mechanism and fits best to the Freundlich isotherm, which supports a multilayer adsorption behavior on a heterogeneous surface. Together, these findings provide comprehensive evidence that the phenol removal by BAC800–2 is governed by a combination of weak, reversible physical interactions rather than chemisorption.

4. Conclusion

This study demonstrates the successful production of high-performance bamboo activated carbon (BAC) using a two-in-one carbonization and activation reactor. The BAC achieved a high surface area (1018 m^2 g^{-1}), > 80 % microporosity, and a pore diameter of 2.08 nm within just 4 h outperforming previous OPKS-AC (935 m^2 g^{-1}, 7 h). BAC800–2 showed excellent phenol removal (>90 % within 15 min at 0.4–0.5 g dosage), surpassing commercial BAC (82.4 % in 60 min). It also performed well across a wide pH range (2–10), aligning with DOE's effluent standards (pH 5–9). The adsorption followed pseudo-first-order kinetics ($R^2 = 0.9995$) and a Freundlich isotherm ($R^2 = 0.9588$), indicating multilayer adsorption. These findings highlight the reactor's efficiency and potential for scalable wastewater treatment applications.

Funding

This research was funded by Universiti Putra Malaysia (UPM) under Geran Putra IPS (GP-IPS/2024/9789300) and Graduate Research Fellowship (GRF). The project also supported by Malaysian Palm Oil Board (MPOB).

Author Statement

We, the undersigned authors, declare that:

1. **Originality**: This manuscript is our original work and has not been published elsewhere in any form nor is it under consideration by any other journal.
2. **Authorship Contributions**: All listed authors have made substantial contributions to the research reported in this manuscript. Specific contributions are as follows:
   - o *Mariam Jamilah Mohd Fairus*: Experimental design, data curation, formal analysis, validation, visualization, and original manuscript writing.
   - o *Mohamad Faizal Ibrahim*: Project administration, conceptualization, supervision, validation, funding acquisition, and manuscript review and editing.
   - o *Nahrul Hayawin Zainal*: Project administration, supervision, validation, funding acquisition, and resources.
   - o *Suraini Abd-Aziz and Phang Lai Yee*: Conceptualization, supervision, validation, and provision of resources.
3. **Approval of Final Version**: All authors have reviewed and approved the final version of the manuscript and agree with its submission to [Journal Name].
4. **Conflict of Interest**: The authors declare no conflict of interest.

5. **Ethical Compliance**: The study did not involve human or animal subjects and complied with all relevant institutional, national, and international guidelines for research integrity.

CRediT authorship contribution statement

Nahrul Hayawin Zainal: Visualization, Validation, Supervision, Resources, Project administration, Methodology, Funding acquisition, Conceptualization. **Abd-Aziz Suraini:** Supervision, Resources. **Phang Lai Yee:** Supervision, Resources. **Mariam Jamilah Mohd Fairus:** Writing – original draft, Visualization, Project administration, Methodology, Investigation, Formal analysis, Data curation. **Mohamad Faizal Ibrahim:** Writing – review & editing, Visualization, Validation, Supervision, Resources, Project administration, Methodology, Funding acquisition, Data curation, Conceptualization.

Declaration of competing interest

The authors declare that they are no financial conflicts of interest or personal relationships that could have influences the work presented in this paper

Acknowledgment

The authors would like to acknowledge support from the collaboration between Malaysia Palm Oil Board (MPOB) and Universiti Putra Malaysia (UPM) for this project.

Data availability

Data will be made available on request.

References

Adeleke, A.O., Omar, R.C., Katibi, K.K., Dele-Afolabi, T.T., Ahmad, A., Quazim, J.O., Amusa, A.A., Alshammari, M.B., 2024. Process optimization of superior biosorption capacity of biogenic oyster shells nanoparticles for Congo red and bromothymol blue dyes removal from aqueous solution: response surface methodology, equilibrium isotherm, kinetic, and reusability studies. Alex. Eng. J. 92, 11–23. https://doi.org/10.1016/j.aej.2024.02.042.

Adewuyi, A., Gennaro, A., Durante, Ch, 2015. Bioadsorbent hura crepitans for the removal of phenol from solution. J. Water Chem. Technol. 37, 277–282. https://doi.org/10.3103/S1063455X1506003X.

Afkhami, A., Saber-Tehrani, M., Bagheri, H., 2010. Simultaneous removal of heavy-metal ions in wastewater samples using nano-alumina modified with 2,4-dinitrophenylhydrazine. J. Hazard Mater. 181, 836–844. https://doi.org/10.1016/j.jhazmat.2010.05.089.

Afsharnia, M., Saeidi, M., Zarei, A., Narooie, M.R., Biglari, H., 2016. Phenol removal from aqueous environment by adsorption onto pomegranate peel carbon. Electron Physician 8, 3248–3256. https://doi.org/10.19082/3248.

Ahmad Juanda, N.I. binti, Md Saleh, N., Nor Yuliana Yuhana, N.Y.Y., Asman, S., Yusoff, F., 2023. Analysis of methylphenol concentration in selangor rivers, Malaysia using solid phase extraction technique coupled with UV-Vis spectroscopy. Sains Malays. 52, 1453–1468. https://doi.org/10.17576/jsm-2023-5205-10.

AL-Doury, M.M.I., Alwan, M.H., 2021. Phenol removal from synthetic wastewater by adsorption column. IOP Conf. Ser. Mater. Sci. Eng. 1058, 012034. https://doi.org/10.1088/1757-899X/1058/1/012034.

de Almeida.F. da Silva Brito. G., Oliveira. R., Grisolia. C., Guirra. L., Weber. I., Evaluation of advanced oxidative processes in biodiesel wastewater treatment, J Photochem Photobiol A Chem 375 (2019) 85–90. https://doi.org/10.1016/j.jphotochem.2019.01.013.

Barrett, E.P., Joyner, L.G., Halenda, P.P., 1951. The determination of pore volume and area distributions in porous substances. I. computations from nitrogen isotherms. J. Am. Chem. Soc. 73, 373–380. https://doi.org/10.1021/ja01145a126.

Bernama, 2023. National bamboo industry development action plan 2021-2030. MalayMail.

Cagnon, B., Py, X., Guillot, A., Stoeckli, F., Chambat, G., 2009. Contributions of hemicellulose, cellulose and lignin to the mass and the porous properties of chars and steam activated carbons from various lignocellulosic precursors. Bioresour. Technol. 100, 292–298. https://doi.org/10.1016/j.biortech.2008.06.009.

Chaowana, P., 2013. Bamboo: an alternative raw material for wood and Wood-Based composites. J. Mater. Sci. Res. 2. https://doi.org/10.5539/jmsr.v2n2p90.

Chen, Y., Wang, D., Wang, X., Wu, J., Song, S., 2025. Enhanced adsorption of phenol using EDTA-4Na- and KOH-modified almond shell biochar. Sustain. Environ. Res. 35 (1), 4.

Cheng, L., Adhikari, S., Wang, Z., Ding, Y., 2015. Characterization of bamboo species at different ages and bio-oil production. J. Anal. Appl. Pyrolysis 116, 215–222. https://doi.org/10.1016/j.jaap.2015.09.008.

Cheung, C.W., Porter, J.F., McKay, G., 2000. Elovich equation and modified Second-Order equation for sorption of cadmium ions onto bone char. J. Chem. Technol. Biotechnol. 75, 963–970. https://doi.org/10.1002/1097-4660(200011)75:11<963::AID-JCTB302>3.0.CO;2-Z.

Csavdari, A.A., 2023. Detailed kinetics of a diffusion driven adsorption process. Stud. Univ. BabeșBolyai Chem. 68, 179–189. https://doi.org/10.24193/subbchem.2023.3.12.

Dasgupta, J., Kumar, A., Mandal, D.D., Mandal, T., Datta, S., 2016. Removal of phenol from aqueous solutions using adsorbents derived from low-cost agro-residues. Desalin. Water Treat. 57, 14188–14212. https://doi.org/10.1080/19443994.2015.1061455.

Dawodu, F.A., Onuh, C.U., Akpomie, K.G., Unuabonah, E.I., 2019. Synthesis of silver nanoparticle from vigna unguiculata stem as adsorbent for malachite Green in a batch system. SN Appl. Sci. 1, 346. https://doi.org/10.1007/s42452-019-0353-3.

De, M., Azargohar, R., Dalai, A.K., Shewchuk, S.R., 2013. Mercury removal by Bio-char based modified activated carbons. Fuel 103, 570–578. https://doi.org/10.1016/j.fuel.2012.08.011.

Demirbas, A., 2004. Effect of initial moisture content on the yields of oily products from pyrolysis of biomass. J. Anal. Appl. Pyrolysis 71, 803–815. https://doi.org/10.1016/j.jaap.2003.10.008.

Dizbay-Onat, M., Vaidya, U.K., Balanay, J.A.G., Lungu, C.T., 2018. Preparation and characterization of flax, hemp and sisal Fiber-Derived mesoporous activated carbon adsorbents. Adsorpt. Sci. Technol. 36, 441–457. https://doi.org/10.1177/0263617417700635.

Djelloul, C., Hasseine, A., Hamdaoui, O., 2017. Adsorption of cationic dye from aqueous solution by milk thistle seeds: isotherm, kinetic and thermodynamic studies. Desalin. Water Treat. 78, 313–320. https://doi.org/10.5004/dwt.2017.20920.

El-Bery, H.M., Saleh, M., El-Gendy, R.A., Saleh, M.R., Thabet, S.M., 2022. High adsorption capacity of phenol and methylene blue using activated carbon derived from lignocellulosic agriculture wastes. Sci. Rep. 12, 5499. https://doi.org/10.1038/s41598-022-09475-4.

Department of Environment, 2020. Environmental Quality Report (2020), Selangor, Malaysia. ⟨https://enviro2.doe.gov.my/ekmc/wp-content/uploads/2021/09/EQR-2020-1.pdf⟩ (accessed December 19, 2024).
Environment and Climate Change Canada (ECCC), Substance list: National Pollutant Release Inventory, Canada, 2022. ⟨https://www.canada.ca/en/environment-climate-change/services/national-pollutant-release-inventory/substances-list.html⟩ (accessed February 26, 2024).
Environmental Protection Agency (EPA), Emergency Planning and Community Right-to-Know Act (EPCRA) Section 313 Chemical list for reporting year 2014, (2023). ⟨https://www.epa.gov/toxics-release-inventory-tri-program/tri-chemical-list-ry-2014-including-toxic-chemical-categories⟩ (accessed February 26, 2024).
El-Gawad, H.A., Hussein, M.H., Zahran, H.A., Kadry, G., 2025. Enhanced phenol removal from wastewater via sulfuric acid activated eggshell derived carbon. Sci. Rep. 15 (1), 20128.
Fathiganjehlou, A., Peters, E.A.J.F., Buist, K.A., Kuipers, J.A.M., 2024. Pore network modeling of intraparticle transport phenomena accompanied by chemical reactions. Ind. Eng. Chem. Res. https://doi.org/10.1021/acs.iecr.4c01727.
Fatriasari, W., Syafii, W., J Wistara, N., Syamsu, K., Prasetya, B., 2014. The characteristic changes of betung bamboo (Dendrocalamus asper) pretreated by fungal pretreatment. Int. J. Renew. Energy Dev. 3, 133–143. https://doi.org/10.14710/ijred.3.2.133-143.
Ferreiro, C., de Luis, A., Villota, N., Lomas, J., Lombraña, J., Camarero, L., 2021. Application of a combined Adsorption−Ozonation process for phenolic wastewater treatment in a continuous Fixed-Bed reactor. Catalysts 11, 1014. https://doi.org/10.3390/catal11081014.
Freundlich, H., 1906. Over the adsorption in solution. J. Phys. Chem. 57, 385–471.
Gabr, S.S., Mubarak, M.F., Keshawy, M., Abdel Moghny, T., El Sayed, I.E.T., 2023. Intensifying of phenol removal from aqueous solutions using ACTF as a hybrid carbon nanostructure: isotherms, kinetics and thermodynamics study. J. Dispers. Sci. Technol. 1–15. https://doi.org/10.1080/01932691.2023.2272756.
Ge, M., Wang, X., Du, M., Liang, G., Hu, G., J. S.M, 2018. Adsorption analyses of phenol from aqueous solutions using magadiite modified with Organo-Functional groups: kinetic and equilibrium studies. Materials 12, 96. https://doi.org/10.3390/ma12010096.
Gök, Ö., Özcan, A., Erdem, B., Özcan, A.S., 2008. Prediction of the kinetics, equilibrium and thermodynamic parameters of adsorption of copper (II) ions onto 8-hydroxy quinoline immobilized bentonite. Colloids Surf. A Physicochem Eng. Asp. 317, 174–185. https://doi.org/10.1016/j.colsurfa.2007.10.009.
Ho, S., 2022. Low-Cost adsorbents for the removal of Phenol/Phenolics, pesticides, and dyes from wastewater systems: a review. Water (Basel) 14, 3203. https://doi.org/10.3390/w14203203.
Ho, Y.S., 1995. Adsorption of heavy metals from waste streams by peat. University of Bermingham.
Hock, P.E., Zaini, M.A.A., 2018. Activated carbons by zinc chloride activation for dye removal – a commentary. Acta Chim. Slov. 11, 99–106. https://doi.org/10.2478/acs-2018-0015.
Hu, Q., Ma, S., He, Z., Liu, H., Pei, X., 2024. A revisit on intraparticle diffusion models with analytical solutions: underlying assumption, application scope and solving method. J. Water Process Eng. 60, 105241. https://doi.org/10.1016/j.jwpe.2024.105241.
Ingole, R.S., Lataye, D.H., Dhorabe, P.T., 2017. Adsorption of phenol onto banana peels activated carbon. KSCE J. Civ. Eng. 21, 100–110. https://doi.org/10.1007/s12205-016-0101-9.
M. Ioelovich, Methods For Determination of Chemical Composition Of Plant Biomass, 2015.
Jabit, N.B., 2007. The production and characterization of activated carbon using local agricultural waste through chemical activation process. Ind. Crops Prod. 23, 23–28.
Jablonsky, M., Haz, A., Jablonský, M., Orságová, A., Botková, A., Šmatko, M., 2013. Relationships between elemental carbon contents and heating values of lignins. Tatranské Matliare Renew. Energy Sources 67–72. ⟨https://www.researchgate.net/publication/236889812⟩.
Jagtoyen, M., Derbyshire, F., 1998. Activated carbons from yellow poplar and White oak by H_3PO_4 activation. Carbon N. Y 36, 1085–1097. https://doi.org/10.1016/S0008-6223(98)00082-7.
Jibril, B.Y., Al-Maamari, R.S., Hegde, G., Al-Mandhary, N., Houache, O., 2007. Effects of feedstock pre-drying on carbonization of KOH-mixed bituminous coal in preparation of activated carbon. J. Anal. Appl. Pyrolysis 80 (2), 277–282.
Kazemi, P., Peydayesh, M., Bandegi, A., Mohammadi, T., Bakhtiari, O., 2014. Stability and extraction study of phenolic wastewater treatment by supported liquid membrane using tributyl phosphate and sesame oil as liquid membrane. Chem. Eng. Res. Des. 92, 375–383. https://doi.org/10.1016/j.cherd.2013.07.023.
Khater, E.-S., Bahnasawy, A., Hamouda, R., Sabahy, A., Abbas, W., Morsy, O.M., 2024. Biochar production under different pyrolysis temperatures with different types of agricultural wastes. Sci. Rep. 14, 2625. https://doi.org/10.1038/s41598-024-52336-5.
Khuong, D.A., Nguyen, H.N., Tsubota, T., 2021. Activated carbon produced from bamboo and solid residue by CO_2 activation utilized as CO_2 adsorbents. Biomass.. Bioenergy 148, 106039. https://doi.org/10.1016/j.biombioe.2021.106039.
Kilic, M., Apaydin-Varol, E., Pütün, A.E., 2011. Adsorptive removal of phenol from aqueous solutions on activated carbon prepared from tobacco residues: equilibrium, kinetics and thermodynamics. J. Hazard Mater. 189, 397–403. https://doi.org/10.1016/j.jhazmat.2011.02.051.
Kumar Shetty, M., Karthik, K.V., Patil, J.H., Murthy Shekhar, S., 2022. Equilibrium removal, isotherm and kinetic studies of chromium (VI) adsorption onto biopolymers from aqueous solution: a comparative study. Mater. Today Proc. 49, 891–897. https://doi.org/10.1016/j.matpr.2021.06.199.
Kuttiraja, M., Sindhu, R., Varghese, P.E., Sandhya, S.V., Binod, P., Vani, S., Pandey, A., Sukumaran, R.K., 2013. Bioethanol production from bamboo (Dendrocalamus sp.) process waste. Biomass.. Bioenergy 59, 142–150. https://doi.org/10.1016/j.biombioe.2013.10.015.
Lagergren, S., 1898. About the theory of So-Called adsorption of soluble substances. K. Sven. Vetensk. Handl. 24, 1–39.
Langmuir, I., 1916. The constitution and fundamental properties of solid and liquids. Part I. Solids. J. Am. Chem. Soc. 38, 2221–2295. https://doi.org/10.1021/ja02268a002.
Leenakul, W., Tippayawong, N., 2010. Dilute acid pretreatment of bamboo for fermentable sugar production. J. Sustain. Energy Environ. 1, 117–120.
León, M., Silva, J., Carrasco, S., Barrientos, N., 2020. Design, cost estimation and sensitivity analysis for a production process of activated carbon from waste nutshells by physical activation. Processes 8, 945. https://doi.org/10.3390/pr8080945.
Li, L.-J., Wang, Y.-P., Wang, G., Cheng, H.-T., Han, X.-J., 2010. Evaluation of properties of natural bamboo fiber for application in summer textiles. J. Fiber Bioeng. Inform. 3, 94–99.
Liang, D., Xie, Q., Liu, J., Xie, F., Liu, D., Wan, C., 2020. Mechanism of the evolution of pore structure during the preparation of activated carbon from zhundong High-Alkali coal based on Gas–Solid diffusion and activation reactions. RSC Adv. 10, 33566–33575. https://doi.org/10.1039/D0RA06105K.
Lu, G., Hao, J., Liu, L., Ma, H., Fang, Q., Wu, L., Wei, M., Zhang, Y., 2011. The adsorption of phenol by lignite activated carbon. Chin. J. Chem. Eng. 19, 380–385. https://doi.org/10.1016/S1004-9541(09)60224-X.
Lua, A.C., 2024. A comparative study of the pore characteristics and phenol adsorption performance of activated carbons prepared from Oil-Palm shell wastes by steam and combined Steam-Chemical activation. Green. Chem. Eng. 5, 85–96. https://doi.org/10.1016/j.gce.2022.11.004.
Lütke, S.F., Igansi, A.V., Pegoraro, L., Dotto, G.L., Pinto, L.A.A., Cadaval, T.R.S., 2019. Preparation of activated carbon from black wattle bark waste and its application for phenol adsorption. J. Environ. Chem. Eng. 7, 103396. https://doi.org/10.1016/j.jece.2019.103396.
Mashhadimoslem, H., Maleki, F., Khosrowshahi, M.S., 2024. Modeling of polymeric adsorbent behavior. in: Polymeric Adsorbents. Elsevier, pp. 393–432. https://doi.org/10.1016/B978-0-323-99746-1.00010-0.
Mohammadi, S., Kargari, A., Sanaeepur, H., Abbassian, K., Najafi, A., Mofarrah, E., 2015. Phenol removal from industrial wastewaters: a short review. Desalin. Water Treat. 53, 2215–2234. https://doi.org/10.1080/19443994.2014.883327.
Mohanty, K., Das, D., Biswas, M.N., 2005. Adsorption of phenol from aqueous solutions using activated carbons prepared from tectona grandis sawdust by $ZnCl_2$ activation. Chem. Eng. J. 115, 121–131. https://doi.org/10.1016/j.cej.2005.09.016.
Molina-Sabio, M., Gonzalez, M.T., Rodriguez-Reinoso, F., Sepúlveda-Escribano, A., 1996. Effect of steam and carbon dioxide activation in the micropore size distribution of activated carbon. Carbon N. Y 34, 505–509. https://doi.org/10.1016/0008-6223(96)00006-1.
Moliner, C., Focacci, S., Antonucci, B., Moreno, A., Biti, S., Hamzah, F., Martinez-Felipe, A., Arato, E., Fernández Martín, C., 2022. Production, activation and CO_2 uptake capacity of a carbonaceous microporous material from palm oil residues. Energ. (Basel) 15, 9160. https://doi.org/10.3390/en15239160.
Nahrul Hayawin, Z., Aziz, A.A., Idris, J., Jalani, N.F., Mamat, R., Ibrahim, M.F., Hassan, M.A., Abd-Aziz, S., 2018. Reduction of POME final discharge residual using activated bioadsorbent from oil palm kernel shell. J. Clean. Prod. 182, 830–837. https://doi.org/10.1016/j.jclepro.2018.02.110.

Naiya, T.K., Bhattacharya, A.K., Das, S.K., 2009. Clarified sludge (basic oxygen furnace sludge) – an adsorbent for removal of Pb(II) from aqueous solutions – kinetics, thermodynamics and desorption studies. J. Hazard Mater. 170, 252–262. https://doi.org/10.1016/j.jhazmat.2009.04.103.
Neziri, E., Duranoğlu, D., 2024. Kinetic, equilibrium, and thermodynamic aspects of phenol adsorption onto acrylonitrile-divinylbenzene copolymer. Sci. Total Environ. 954, 176710. https://doi.org/10.1016/j.scitotenv.2024.176710.
Pal, A., Uddin, K., Saha, B.B., Thu, K., Kil, H.-S., Yoon, S.-H., Miyawaki, J., 2020. A benchmark for CO_2 uptake onto newly synthesized biomass-derived activated carbons. Appl. Energy 264, 114720. https://doi.org/10.1016/j.apenergy.2020.114720.
Pallarés, J., González-Cencerrado, A., Arauzo, I., 2018b. Production and characterization of activated carbon from barley straw by physical activation with carbon dioxide and steam. Biomass.. Bioenergy 115, 64–73. https://doi.org/10.1016/j.biombioe.2018.04.015.
Pallarés, J., González-Cencerrado, A., Arauzo, I., 2018a. Production and characterization of activated carbon from barley straw by physical activation with carbon dioxide and steam. Biomass.. Bioenergy 115, 64–73. https://doi.org/10.1016/j.biombioe.2018.04.015.
Phothong, K., Tangsathitkulchai, C., Lawtae, P., 2021. The analysis of pore development and formation of surface functional groups in Bamboo-Based activated carbon during CO_2 activation. Molecules 26, 5641. https://doi.org/10.3390/molecules26185641.
Plazinski, W., Rudzinski, W., 2009. Kinetics of adsorption at Solid/Solution interfaces controlled by intraparticle diffusion: a theoretical analysis. J. Phys. Chem. C. 113, 12495–12501. https://doi.org/10.1021/jp902914z.
Pradeep, N.V., Anupama, S., Navya, K., Shalini, H.N., Idris, M., Hampannavar, U.S., 2015. Biological removal of phenol from wastewaters: a mini review. Appl. Water Sci. 5, 105–112. https://doi.org/10.1007/s13201-014-0176-8.
Rennhofer, H., Köhnke, J., Keckes, J., Tintner, J., Unterweger, C., Zinn, T., Deix, K., Lichtenegger, H., Gindl-Altmutter, W., 2021. Pore development during the carbonization process of lignin microparticles investigated by small angle X-ray scattering. Molecules 26, 2087. https://doi.org/10.3390/molecules26072087.
Rini, D.S., Ishiguri, F., Nezu, I., Ngadianto, A., Irawati, D., Otani, N., Ohshima, J., Yokota, S., 2023. Geographic and longitudinal variations of anatomical characteristics and mechanical properties in three bamboo species naturally grown in lombok island, Indonesia. Sci. Rep. 13, 2265. https://doi.org/10.1038/s41598-023-29288-3.
Rudzinski, W., Plazinski, W., 2006. Kinetics of solute adsorption at Solid/Solution interfaces: a theoretical development of the empirical Pseudo-First and Pseudo-Second order kinetic rate equations, based on applying the statistical rate theory of interfacial transport. J. Phys. Chem. B 110, 16514–16525. https://doi.org/10.1021/jp061779n.
Saleh, T.A., 2022. Kinetic models and thermodynamics of adsorption processes: classification. Interf. Sci. Technol. 65–97. https://doi.org/10.1016/B978-0-12-849876-7.00003-8.
Saputera, W.H., Putrie, A.S., Esmailpour, A.A., Sasongko, D., Suendo, V., Mukti, R.R., 2021. Technology advances in phenol removals: current progress and future perspectives. Catalysts 11, 998. https://doi.org/10.3390/catal11080998.
Sazali, N., Harun, Z., Sazali, N., 2020. A review on batch and column adsorption of various adsorbent towards the removal of heavy metal. J. Adv. Res. Fluid Mech. Therm. Sci. J. Homepage 67, 66–88. ⟨www.akademiabaru.com/arfmts.html⟩.
Sparks, D.L., Singh, B., Siebecker, M.G., 2024. Sorption phenomena on soils. in: Environmental Soil Chemistry. Elsevier, pp. 203–281. https://doi.org/10.1016/B978-0-443-14034-1.00005-8.
Srivastava, V.C., Mall, I.D., Mishra, I.M., 2006. Characterization of mesoporous rice husk ash (RHA) and adsorption kinetics of metal ions from aqueous solution onto RHA. J. Hazard Mater. 134, 257–267. https://doi.org/10.1016/j.jhazmat.2005.11.052.
Subyakto, S., Budiman, I., Pari, G., 2017. Effects of temperature and time of carbonization on the properties of bamboo (Dendrocalamus asper) carbon. Wood Res. J. 4, 68–73. https://doi.org/10.51850/wrj.2012.3.2.68-73.
M. Sudibandriyo, M. Oratmangun, Betung Bamboo-Based Activated Carbon Bioadsorbent for the Separation of Hydrogen-Methane Gas Mixture, in: E3S Web of Conferences, EDP Sciences, 2018. https://doi.org/10.1051/e3sconf/20186702039.
Sun, J., Liu, X., Zhang, F., Zhou, J., Wu, J., Alsaedi, A., Hayat, T., Li, J., 2019. Insight into the mechanism of adsorption of phenol and resorcinol on activated carbons with different oxidation degrees. Colloids Surf. A Physicochem Eng. Asp. 563, 22–30. https://doi.org/10.1016/j.colsurfa.2018.11.042.
Sun, X., Wang, C., Li, Y., Wang, W., Wei, J., 2015. Treatment of phenolic wastewater by combined UF and NF/RO processes. Desalination 355, 68–74. https://doi.org/10.1016/j.desal.2014.10.018.
Sun, Z.-Y., Tang, Y.-Q., Iwanaga, T., Sho, T., Kida, K., 2011. Production of fuel ethanol from bamboo by concentrated sulfuric acid hydrolysis followed by continuous ethanol fermentation. Bioresour. Technol. 102, 10929–10935. https://doi.org/10.1016/j.biortech.2011.09.071.
Surela, A.K., Chhachhia, L.K., Surela, V.K., Meena, P.L., 2024. Polypyrrole-Based composites for dyes removal from contaminated water. in: Reference Module in Materials Science and Materials Engineering. Elsevier. https://doi.org/10.1016/B978-0-323-95486-0.00019-3.
Suresh Babu, K.K.B., Nataraj, M., Tayappa, M., Vyas, Y., Mishra, R.K., Acharya, B., 2024. Production of biochar from waste biomass using slow pyrolysis: studies of the effect of pyrolysis temperature and holding time on biochar yield and properties. Mater. Sci. Energy Technol. 7, 318–334. https://doi.org/10.1016/j.mset.2024.05.002.
Tan, Y.Y., Bello, M.M., Abdul Raman, A.A., 2021. Towards cleaner production in palm oil industry: advanced treatment of Biologically-Treated POME using palm kernel Shell-Based adsorbent. Clean. Eng. Technol. 2, 100079. https://doi.org/10.1016/j.clet.2021.100079.
Taraba, B., Bulavová, P., 2018. Adsorption enthalpy of lead (II) and phenol on coals and activated carbon in the view of thermodynamic analysis and calorimetric measurements. J. Chem. Thermodyn. 116, 97–106. https://doi.org/10.1016/j.jct.2017.08.026.
Temkin, M., Pyzhev, V., 1940. Kinetics of ammonia synthesis on promoted iron catalysts. Acta Physicochim. U. R. S. S 12, 327–356.
Thommes, M., Kaneko, K., Neimark, A.V., Olivier, J.P., Rodriguez-Reinoso, F., Rouquerol, J., Sing, K.S.W., 2015. Physisorption of gases, with special reference to the evaluation of surface area and pore size distribution (IUPAC Technical Report). Pure Appl. Chem. 87, 1051–1069. https://doi.org/10.1515/pac-2014-1117.
Van der Bruggen, B., 2014. Freundlich isotherm. in: Encyclopedia of Membranes. Springer Berlin Heidelberg, Berlin, Heidelberg, pp. 1–2. https://doi.org/10.1007/978-3-642-40872-4_254-3.
S. Varghese, V.P. Vinod, T.S. Anirudhan, Kinetic and equilibrium characterization of phenols adsorption onto a novel activated carbon in water treatment, 2004.
Villegas, L.G.C., Mashhadi, N., Chen, M., Mukherjee, D., Taylor, K.E., Biswas, N., 2016. A short review of techniques for phenol removal from wastewater. Curr. Pollut. Rep. 2, 157–167. https://doi.org/10.1007/s40726-016-0035-3.
Wang, R., Amano, Y., Machida, M., 2013. Surface properties and water vapor adsorption–desorption characteristics of bamboo-based activated carbon. J. Anal. Appl. Pyrolysis 104, 667–674. https://doi.org/10.1016/j.jaap.2013.04.013.
Weber, W.J., Morris, J.C., 1963. Kinetics of adsorption on carbon from solution. J. Sanit. Eng. Div. 89, 31–59. https://doi.org/10.1061/JSEDAI.0000430.
Xie, B., Qin, J., Wang, S., Li, X., Sun, H., Chen, W., 2020. Adsorption of phenol on commercial activated carbons: modelling and interpretation. Int J. Environ. Res Public Health 17, 789. https://doi.org/10.3390/ijerph17030789.
Xing, W., Liu, C., Zhou, Z., Zhang, L., Zhou, J., Zhuo, S., Yan, Z., Gao, H., Wang, G., Qiao, S.Z., 2012. Superior CO_2 uptake of N-doped activated carbon through hydrogen-bonding interaction. Energy Environ. Sci. 5, 7323. https://doi.org/10.1039/c2ee21653a.
Yorgun, S., Yıldız, D., 2015. Preparation and characterization of activated carbons from paulownia wood by chemical activation with H_3PO_4. J. Taiwan Inst. Chem. Eng. 53, 122–131. https://doi.org/10.1016/j.jtice.2015.02.032.
Yu, P., Luo, Z., Wang, Q., Fang, M., Zhou, J., Wang, W., Liang, X., Cai, W., 2020. Activated Carbon-Based CO_2 uptake evaluation at different temperatures: the correlation analysis and coupling effects of the preparation conditions. J. CO_2 Util. 40, 101214. https://doi.org/10.1016/j.jcou.2020.101214.
Zhou, J.-J., Zhang, M., Lu, J., Gu, M.-X., Li, Y.-X., Liu, X.-Q., Sun, L.-B., 2021. Controllable microporous framework isomerism within continuous mesoporous channels: hierarchically porous structure for capture of bulky molecules. Inorg. Chem. 60, 6633–6640. https://doi.org/10.1021/acs.inorgchem.1c00438.
Zulkurnai, N.Z., Md. Ali, U.F., Ibrahim, N., Abdul Manan, N.S., 2017. Carbon dioxide (CO_2) adsorption by activated carbon functionalized with deep eutectic solvent (DES). IOP Conf. Ser. Mater. Sci. Eng. 206, 012001. https://doi.org/10.1088/1757-899X/206/1/012001.

Further reading

Hoseinzadeh, R., Arami-niya, A., Mohd, W., Wan, A., Sahu, J., 2013. Comparison of oil palm shell-based activated carbons produced by microwave and conventional heating methods using zinc chloride activation. J. Anal. Appl. Pyrolysis 104, 176–184. https://doi.org/10.1016/j.jaap.2013.08.006.

Li, W., Zhang, L., Peng, J., Li, N., Zhu, X., 2008. Preparation of high surface area activated carbons from tobacco ttems with K_2CO_3 activation using microwave radiation. Ind. Crops Prod. 27, 341–347. https://doi.org/10.1016/j.indcrop.2007.11.011.